The GTPase activating protein Gyp6 binds Retromer and inactivates Rab7/Ypt7 to coordinate the formation of endosomal carriers

Ana Catarina Alves*[1], Kai-En Chen*[2], Lydie Michaillat Mayer[1], Qian Guo[2], Ella J. Stephens[2], Meihan Liu[2], Michael D. Healy[2], Brett M. Collins*[2], Andreas Mayer*[1]

1. Department of Immunobiology, University of Lausanne, Epalinges, Switzerland.
2. The University of Queensland, Centre for Cell Biology of Chronic Disease, Institute for Molecular Bioscience, St. Lucia, Queensland, Australia.

* These authors contributed equally
e-mail: andreas.mayer@unil.ch, b.collins@imb.uq.edu.au

Keywords: Rab GTPase, Retromer, endosome, GTPase activating protein (GAP), yeast.

Abstract

The Retromer coat is conserved in all eukaryotes and is crucial for the correct intracellular sorting of many transmembrane receptors and lysosomal hydrolases. Retromer is an effector of the late endosomal small GTPase RAB7 and is also implicated in its inactivation required for proper endosomal maturation. Here, we explore the role of controlled GTP hydrolysis by the RAB7 ortholog Ypt7 in the formation of Retromer-coated membrane carriers in yeast. Proximity labelling and genetic ablation identify the GTPase Activating Protein (GAP) Gyp6 as a critical regulator of Ypt7 activity in the context or Retromer. Structural studies show that Retromer recruits Gyp6 through its Vps29 subunit, which recognises a specific PL motif and a secondary binding site in the C-terminal domain of Gyp6. This interaction does not occur with other yeast GAPs. Ablation of the Gyp6-Retromer interface or the catalytic activity of Gyp6 leads to the accumulation of tubular structures on endo-lysosomal compartments and to increased association of Ypt7 with Retromer and its cargo Vps10. These results support a model in which Gyp6 controls the switch from Ypt7-dependent Retromer coat assembly and cargo collection to the departure of the carrier through membrane fission and uncoating.

Introduction

The delivery of transmembrane protein and lipid cargos to specific cellular compartments is an essential process in all eukaryotes and is regulated by a complex network of trafficking pathways. Collectively, these pathways guarantee the distribution of such cargoes to a great variety of specific destinations, which is vital for cellular homeostasis. Disruption or dysregulation of the cargo-trafficking system in humans is associated with various diseases, including neurodegenerative disorders such as Parkinson's and Alzheimer's disease (Panicker *et al*, 2021; Qureshi *et al*, 2020), and infection by bacterial and viral pathogens (Yong *et al*, 2021).

Among the key players on endo-lysosomal compartments is Retromer, a conserved complex of the proteins Vps35, Vps26 and Vps29. Retromer orchestrates the recruitment of cargoes into tubulovesicular carriers, ensuring their escape from the lysosomal degradation system and, thus, their reuse (Seaman, 2012; Gopaldass *et al*, 2024; Yong *et al*, 2022; Chen *et al*, 2019). The molecular stages governing carrier formation involve cargo recognition, Retromer oligomerization, membrane tubulation, membrane fission, and, eventually, uncoating. Recruitment of Retromer to the endosomal membrane precedes or occurs concomitantly with the selection of cargo proteins, requiring adaptors from the sorting nexin (SNX) protein family for cargo recruitment. In yeast, Retromer can form a pentameric assembly with a dimer of Vps5–Vps17, two SNX proteins with bin/amphiphysin/rvs (BAR) domains (Kovtun *et al*, 2018; Chen *et al*, 2025; Gopaldass *et al*, 2023; Seaman *et al*, 1998), or a tetramer with the Snx3 adaptor (Strochlic *et al*, 2007; Purushothaman & Ungermann, 2018; Leneva *et al*, 2021). In each case, Retromer cooperates with the SNX adaptor to bind cargo sequences and promote formation of endosomal membrane tubules into which the cargo proteins are sorted. Following tubule detachment, Retromer should dissociate from the membrane so that further rounds of cargo sorting can occur.

Retromer activity is closely linked to its interaction with small GTPases, particularly RAB7, a member of the Rab family that controls the maturation and fusion of the endosomal sorting compartment with late endosomes/lysosomes (or the vacuole in yeast (Feng *et al*, 1995; Wichmann *et al*, 1992). Rab GTPases function as molecular switches that alternate between

an active GTP-bound state and an inactive GDP-bound state, and regulation of their activity is crucial for maintaining the homeostasis of the late endocytic pathway (Homma *et al*, 2021; Pylypenko *et al*, 2018; Stenmark, 2009; Kummel *et al*, 2023). This Rab switching is controlled by guanine nucleotide exchange factors (GEFs) that swap GDP for GTP to activate the Rab, and by GTPase-activating proteins (GAPs) that enhance GTP hydrolysis and Rab inactivation. The mammalian Retromer complex depends on Rab GTPases for efficient membrane recruitment (Rojas *et al*, 2008; Seaman *et al*, 2009; Modica *et al*, 2025; Priya *et al*, 2015; Harrison *et al*, 2014; Liu *et al*, 2012) and in turn impacts Rab conversion, the replacement of RAB5 by RAB7, at the endosomal compartment (Xie *et al*, 2020; Distefano *et al*, 2018; Jimenez-Orgaz *et al*, 2018; Jia *et al*, 2016; Antón-Plágaro *et al*, 2025). Retromer associates with endosomes partly through its interaction with GTP-bound RAB7. Recruitment of the GAP TBC1D5 promotes RAB7 GTP hydrolysis and inactivation. Blocking this process entails accumulation of active RAB7 and defects in endosomal maturation, which led to the suggestion that GTP-hydrolysis by RAB7 might trigger coat disassembly (Jia *et al*, 2016). However, attempts to manipulate the GAP-stimulated GTP hydrolysis by RAB7 produced inconsistent effects on localisation of endosomal cargoes such as CI-MPR, GLUT1, integrin-α5 and the HPV protein L2 (Seaman *et al*, 2009; Jimenez-Orgaz *et al*, 2018; Xie *et al*, 2020), challenging this idea. In yeast, Retromer associates with the RAB7 orthologue Ypt7 (Balderhaar *et al*, 2010; Liu *et al*, 2012; Purushothaman *et al*, 2017; Wu *et al*, 2021), but no Retromer-associated GAPs have yet been reported. Ypt7 is activated by the Mon1-Ccz1 GEF complex (Nordmann *et al*, 2010), and the yeast GAP Gyp7 regulates Ypt7 activity (Füllbrunn *et al*, 2024; Brett *et al*, 2008; Vollmer *et al*, 1999), although its specificity for RAB substrates is relatively broad *in vitro* (Vollmer *et al*, 1999). Yeast has eleven RABs and eight GAPs, the latter being characterised by a Tre/Bub2/Cdc16 (TBC) domain with a catalytic arginine-glutamine finger. Whether GAPs other than Gyp7 can control Ypt7 activity, and whether any of these might cooperate with Retromer in an analogous way to mammalian TBC1D5, is unknown.

In this study, we used a TurboID-based proteomics approach to identify yeast proteins associated with Ypt7 in its native environment. Combining the results with *in silico* modelling, structural and biochemical studies we show that Gyp6 is the only yeast GAP protein capable of associating with both Retromer and Ypt7 and elucidate its dual mechanism of binding to Retromer. We analysed its impact on Vps10 cargo recycling *in vivo*, on the formation of

endosomal carriers and on Retromer coat complex formation, leading us to a model in which Gyp6 exerts spatiotemporal control over the transition from cargo collection to carrier departure.

Results

RAB7 and its yeast homolog Ypt7 are important for the stable membrane recruitment of Retromer as well as proper maturation of the early endosome into degradative vacuolar and lysosomal compartments (Rojas *et al*, 2008; Seaman *et al*, 2009; Balderhaar *et al*, 2010; Liu *et al*, 2012; Priya *et al*, 2015; Harrison *et al*, 2014; Modica *et al*, 2025; Wu *et al*, 2021). We aimed to examine the role of GTP hydrolysis by Ypt7 in the formation of endosomal carriers in yeast to explore whether Ypt7 might constitute a GTP-triggered switch between different stages of endosomal carrier formation.

Proximity labelling identifies Gyp3 and Gyp6 as potential GAP(s) of Ypt7

In its multiple endo-lysosomal functions, Ypt7 interacts with different partners (Numrich *et al*, 2015; Kucharczyk *et al*, 2001; Balderhaar *et al*, 2010; Cabrera *et al*, 2009). These may be regulated by the actions of different GAPs, but assigning a specific GAP to a specific Ypt7-dependent process is complicated by their potential redundancy (Fukuda, 2011). We therefore investigated the protein-protein interactions with Ypt7 by proximity labelling, which can capture transient and weak GAP-Ypt7 interactions in the native cellular environment. TurboID (a yeast optimized biotin ligase) and a V5 epitope were fused to the *Saccharomyces cerevisiae* (sc) Ypt7 N-terminus and integrated into the URA3 locus of a *ypt7Δ* mutant **(Figure 1A)** (Kim *et al*, 2014; Branon *et al*, 2018). Since expressing this fusion construct from an endogenous YPT7 promoter did not completely rescue the vacuole fragmentation phenotype of a *ypt7Δ* mutant, we expressed TurboID-V5-YPT7 (wild-type or variants) from a tetracycline-inducible promoter. This construct resulted in slightly increased Ypt7 expression levels compared to a wild-type strain (**Supplementary Fig. S1**) and completely rescued the vacuole morphology of *ypt7Δ* cells. As a control, we expressed non-fused Turbo-ID-V5 in the URA3 locus of wildtype cells.

We performed proximity labelling with three alleles of *YPT7*: The *YPT7* wild-type, a *ypt7*^{T22N} allele coding a single amino acid substitution that interferes with GTP binding, and *ypt7*^{Q68L}, which alters the switch II glutamine sidechain and reduces GTPase activity, but maintains a considerable potential for stimulating this activity by GAPs (Vollmer *et al*, 1999). *ypt7*^{Q68L} was expected to stabilize Ypt7-GAP interactions while *ypt7*^{T22N} is expected to impair them. Cells were labelled with biotin, lysed, and biotinylated proteins were enriched on magnetic streptavidin beads and identified by mass spectrometry. The $\log_2$ fold-change (FC) of peptides enriched in extracts from the wildtype TurboID-V5-YPT7 cells relative to those expressing only TurboID-V5 (control) were plotted (**Figure 1A**). Numerous known regulators and interacting partners of Ypt7 were among the best hits in TurboID-V5-Ypt7 cells, validating the approach: Mon1 and Ccz1, which form the GEF of Ypt7 (Nordmann *et al*, 2010), and Gdi1 (GDP dissociation inhibitor) (Garrett *et al*, 1994); the Retromer subunits Vps35, Vps26, and Vps29 (Seaman *et al*, 2009; Balderhaar *et al*, 2010); the HOPS subunits Vam6/Vps39 and Vps41 (acting in vacuole fusion (Seals *et al*, 2000); Ivy1 (a regulator of vacuole membrane homeostasis and nutrient sensing) (Lazar *et al*, 2002; Numrich *et al*, 2015). Along with these proteins, the Rab-GAPs Gyp6 and Gyp3/Msb3 (Albert & Gallwitz, 1999) were biotinylated by TurboID-V5-Ypt7 (**Figure 1B**). Gyp3 and Gyp6 proximity labelling increased significantly in cells carrying *ypt7*^{Q68L}, probably because this variant has lower GTPase activity and hence favours interaction with GAPs. Gyp7, which has been identified as a cognate GAP of Ypt7 in previous studies (Brett *et al*, 2008; Vollmer *et al*, 1999; Stroupe, 2018), was not enriched in our Ypt7 proximity interactome.

We complemented these proteomics findings through *in silico* screening with AlphaFold2-multimer (AF2) (Mirdita *et al*, 2022). Complexes of Ypt7 with candidate proteins from our proximity labelling were predicted, and the confidence of the modelled interactions was assessed via several metrics, including the interfacial PTM (iPTM) score (**Figure 1C**), consistency of the models in AF2 and AlphaFold3 (AF3), and the pDockQ score (**Figures 1D and 1E**). With this approach, we found 19 out of 458 potential Ypt7 interactors with an iPTM score above 0.5, and 10 of these exhibited consistently high confidence scores. Most of these 19 proteins are known Ypt7 interactors (**Supplementary Fig. S2**). Among the top hits are the GAPs Gyp6, Gyp3 as well as Gyp7, which was not detected in our proximity labelling approach but was included in the computational screen due to evidence from previous studies (Brett

et al, 2008; Vollmer *et al*, 1999; Stroupe, 2018). A high confidence interaction was also obtained for Retromer, where Ypt7 is predicted to occupy an N-terminal region on Vps35 (**Figures 1F and 1G**) (Schmid & Walter, 2025).

Gyp6-dependent trafficking of Vps10

Since Rab-GAPs often show redundant activity, we employed two strategies to test the functional significance of Gyp3, Gyp6 and Gyp7 for Ypt7 in the context of Retromer-dependent trafficking *in vivo*. To address potential redundancy, we ablated Gyp3, Gyp6 and Gyp7 individually and in combinations in *S. cerevisiae*. Their relationship to Ypt7 was probed through the *ypt7*^{Q68L} allele, which has 5-fold reduced GTPase activity but can still be stimulated by GAPs (Vollmer *et al*, 1999). It can hence provide a sensitized background for probing the effect of GAPs on sorting of Retromer cargo *in vivo*. We categorized the mutants according to the fraction of cells that accumulated the Retromer cargo Vps10 fused with mNeonGreen (Vps10^{mNG}) on the (FM 4-64-labeled) vacuolar membrane (**Figures 2A and 2B**). Vps10^{mNG} was detected on vacuoles in less than 2% of all YPT7 wildtype cells, and this proportion remained low in the *ypt7*^{Q68L} strain (5% of all cells). Both *gyp3Δ* and *gyp6Δ* single mutants and *gyp6Δ gyp3Δ* double mutants were very responsive to the presence of *ypt7*^{Q68L}. Introducing *ypt7*^{Q68L} into *gyp6Δ* cells increased the fraction showing vacuolar Vps10^{mNG} from 10% to 35%; for *gyp6Δ gyp3Δ* the fraction increased from 63% to 100% (**Figures 2A and 2B**). The *gyp6Δ gyp3Δ ypt7*^{Q68L} cells thus phenocopied the strong sorting defect of the Retromer mutant *vps35Δ*. *gyp7Δ* cells showed no impact on Vps10^{mNG} localization, neither alone nor in all possible combinations with *gyp3Δ, gyp6Δ* and *ypt7*^{Q68L} mutations **(Supplementary Figures S3, S4A and S4B)**. Gyp6 also affected a phenotype that is linked to the missorting of Vps10, the secretion of the vacuolar hydrolase carboxypeptidase Y. *gyp6Δ* cells secreted significantly more carboxypeptidase Y than wildtype and *gyp3Δ* cells, and *gyp3Δ gyp6Δ* revealed a strong additive effect **(Figure 2C).**

To further explore how these GAP family members might link to Retromer and Ypt7, we performed an *in silico* screen of all nine yeast Rab GAPs against the three individual Retromer subunits using both AF2 and AF3. The confidence of the binding models was ranked by combining iPTM scores from the AF runs with the pDockQ score as mentioned above. Among

the nine *S. cerevisiae* GAPs screened, Gyp6 showed the highest predicted interaction scores, preferentially associating with Vps29 and Vps35 (**Figure 2D; Supplementary Fig. S5A-S5B**). For the interaction with Ypt7, AlphaFold models predict that Gyp6 binds to the expected surface patch of Ypt7 (**Supplementary Fig. S5C-S5D**), inserting its canonical Arginine finger (Arg155) to enable GAP activity (**Supplementary Fig. S5E**). To confirm that Gyp6 functions as a GAP for Ypt7, we assessed GTPase activity using the GTPase-Glo^{TM} assay. Here, GAP activity was tested using Gyp6 from both *S. cerevisiae* and *Chaetomium thermophilum* to assess conservation across different yeast species. Using the recombinant full-length Gyp6, we observed robust activation of Ypt7 (**Figure 2E**) with GAP activity increasing in a concentration dependent manner (**Figure 2F**). Similar *in vitro* GAP activity was also observed using the *C. thermophilum* homologues, Gyp6-like protein TBC domain (ctGyp6L^{TBC}) and ctYpt7. Wild-type ctGyp6L^{TBC} strongly activated the GTPase activity of ctYpt7 (**Figure 2G**). In contrast, the ctGyp6L^{TBC} R129A/Q229A mutant, where the conserved arginine finger and the YxQ motif that are necessary for GAP activity were substituted (Pan *et al*, 2006), showed no detectable activity (**Figure 2G**). While the *C. thermophilum* GAPs ctGyp7^{TBC} and ctGyp6L^{TBC} both displayed significant GAP activity, activation by ctGyp3^{TBC} was weaker (**Figure 2H**). In combination with its strong signal in proximity labelling, its impact on Vps10 sorting, and confidently predicted interaction using AlphaFold, these observations suggest Gyp6 as the preferred GAP for Ypt7 in the context of Retromer activity. In line with this, Gyp6 also localizes to dot-like structures, where we found a Gyp6^{mNG} fusion protein to frequently colocalize with Vps35^{mCherry} in puncta (**Supplementary Fig. S6**), which are likely to represent endosomal compartments (Ali *et al*, 2004; Suda *et al*, 2013; Brunet *et al*, 2016; Thomas *et al*, 2021).

Gyp6 interacts with Retromer via a PL-motif

Predictions of the *S. cerevisiae* Retromer–Gyp6 complex using AF3 indicate that two regions of the Retromer trimer are involved in the interaction (**Figure 3A; Supplementary Fig. S7A-S7C**). According to the models, a high confidence interaction is observed between Vps29 and a Pro-Leu (PL) motif of Gyp6, which is located within the long hinge loop (Leu48 to Leu142) next to the arginine finger of the TBC domain (**Figures 3A, 3B, 3C and 3D**). Such PL-motifs are a frequent feature of Vps29-binding proteins across evolution (Antón-Plágaro *et al*, 2025; Guo *et al*, 2024; Healy *et al*, 2023; Yao *et al*, 2018; Romano-Moreno *et al*, 2017; Barlocher *et al*, 2017; Crawley-Snowdon *et al*, 2020). This PL motif is unique to Gyp6 among yeast Rab GAPs

(**Figure 3E**) but it is conserved across Gyp6 homologs in different yeast species (**Figure 3F**). Confident predictions of PL-mediated Gyp6-Retromer interactions were also obtained for the *C. thermophilum* and *S. pombe* orthologs (**Supplementary Fig. S8**). However, the PL motif in ctGyp6L and spGyp6 is located on a shorter loop between helix 4 and helix 5 of the TBC domain, in contrast to the longer loop found in *S. cerevisiae* Gyp6 (**Supplementary Fig. S8**).

To validate the AlphaFold models, we confirmed the contribution of the PL motif to the Gyp6-Retromer interaction by isothermal calorimetry (ITC) and X-ray crystallography. Due to challenges in producing sufficient *S. cerevisiae* Retromer subunits for ITC and structural studies, we used *C. thermophilum* and human Retromer subunits for these experiments. Using ITC, we found that a Gyp6$^{105\text{-}122}$ peptide containing the PL motif binds to ctVps29 with a K_d of 1.4 µM (**Figure 3G; Table 1**). Under the same condition, we found the recombinant ctGyp6L^{TBC} binds to ctVps29 with a K_d of 27 µM, but the PL motif containing peptide, ctGyp6L$^{87\text{-}107}$ failed to interact due to the weaker affinity (**Figure 3G; Supplementary Fig. 9, Table 1**). In both cases, binding could be abolished by a known competitive Vps29 inhibitor, the cyclic peptide RT-D3 (Chen *et al*, 2021), which also contains a PL motif able to outcompete other proteins requiring the same site in Vps29 (**Figure 3G**). This confirms that the PL motif is required for the Gyp6-Vps29 interaction.

Next, we attempted to obtain the crystal structure of Vps29 in complex with Gyp6 or Gyp6-derived peptides. From multiple crystallization screens, diffraction-quality crystals were obtained using a combination of mouse VPS29 (mVPS29) in complex with *S. cerevisiae* Gyp6$^{105\text{-}122}$ and ctGyp6L$^{87\text{-}107}$ peptides. In the case of the Gyp6$^{105\text{-}122}$ peptide complex, the structure was solved at 1.9 Å resolution (**Table 2**) with the peptide density from Val112 to Asp122 of Gyp6 clearly visible (**Figure 3H**). The region upstream of the PL motif (residues Val112 to His118) contributes to binding, including a charge interaction between Glu113 of Gyp6 and Lys276 of Vps29 (Arg176 in mouse VPS29) (**Figure 3I**). The AlphaFold models of the *S. cerevisiae* proteins correspond well with this crystal structure. In addition, they provide information on the N-terminal part of the Gyp6$^{105\text{-}122}$ peptide that is not resolved in the crystal structure (**Figure 3I**). These models suggest that further residues upstream of the PL motif may be involved in binding, with Val100, Val104, Ile105, and Leu109 providing hydrophobic interactions with residues on Vps29 and in the Vps29–Vps35 interface.

The structures suggest two distinct PL motif binding modes. The ctGyp6L interaction involves a PL motif within a short loop region that binds Vps29 (**Figures 3K and 3L**). This short loop links two flanking helices that are tightly associated through hydrophobic interactions, forming a β-hairpin (**Figure 3L**). This arrangement resembles that of TBC1D5 binding to VPS29 **(Figure 3M)** (Jia *et al*, 2016). In this binding mode, the PL motif is the main region responsible for the contact and the interaction is weaker. By contrast, the interaction of *S. cerevisiae* Gyp6 with Vps29 shows a longer hinge loop in which additional residues reinforce the binding (**Figure 3M**). In the crystal structure of the isolated ctGyp6L^{TBC} domain, electron density was not observed for the loop containing the PL motif, suggesting it is flexible in the absence of Vps29 interaction (**Supplementary Fig. S10A-S10B**). Overall, our structural data show that Gyp6 from different yeast species shares a conserved PL motif to bind to Vps29, but the *S. cerevisiae* protein has additional contacts with Retromer that explain its higher binding affinity.

The C-terminal tail of Gyp6 provides a second Retromer interaction site

Further analysis of the Gyp6 proteins and their interactions with Retromer revealed that Gyp6L from *C. thermophilum* contains a long, disordered C-terminal tail that is not present in *S. cerevisiae* Gyp6 (**Figure 4A**). In the ctRetromer–ctGyp6L complex Alphafold model, this disordered C-terminal tail (residues Gly676 to Gly773) binds to the rear side of the ctVps35 α-helical solenoid (**Figure 4B**). This interaction involves several Leu, Ile, and Phe residues within the disordered ctGyp6L tail, and is conserved among related species (**Figures 4C; Supplementary Fig. S11**). Interestingly, this resembles the interaction between human VPS35 and the LFa repeat motifs of human FAM21 (**Figure 4D**) (Guo *et al*, 2024). These LFa motifs in FAM21 have an inherently low affinity for human VPS35 (Guo *et al*, 2024), and we were similarly unable to measure a K_d of ctRetromer binding to synthetic peptides of the ctGyp6L tail region by ITC (residues 680-698 and 760-773) (**Figure 4E**). It is possible that the multiple LFa-like motifs ctGyp6L (we refer these as 'LFa-like' due to the absence of clustered acidic residues) in the tail must cooperate with each other and with the canonical PL-motif interaction with Vps29 to enhance avidity for Retromer. To test this, we designed a scaffold to artificially increase the number of LFa-like sequences by fusing the C-terminal tail of ctGyp6L (residues 676 to 773, containing three LFa-like motifs) to the C-terminus of the archaeal

protein Lsm alpha (LsmA). This protein assembles into highly stable homo-hexameric and heptameric ring structures (**Supplementary Fig. S12A-S12E**) (Collins *et al*, 2001). Using mass photometry, we found that the chimeric construct, LsmA-ctGyp6L$^{676-773}$, adopts a size consistent with a hexamer (**Supplementary Fig. S12F**), indicating that the addition of ctGyp6L$^{676-773}$ does not alter the oligomerization state of LsmA. We then performed ITC experiments of LsmA-ctGyp6L$^{676-773}$ with ctRetromer. The chimeric protein showed enhanced binding affinity with a K_d of 5.8 µM (**Figure 4F; Table 1**). In contrast, a mutant construct with the LFa-like motifs substituted to alanine showed no detectable binding (**Figure 4F**), confirming that the C-terminal tail of ctGyp6L binds to the ctVps35 subunit of ctRetromer through its LFa-like motif.

In the case of *S. cerevisiae* Gyp6, the C-terminal tail is much shorter than that of *C. thermophilum* Gyp6 and is instead predicted to form an α-helix (**Figure 4A**). According to AF3 modelling, this α-helical C-terminus may bind at the Vps26–Vps35 interface through several conserved charged and hydrophobic residues (**Figures 4G-4H; Supplementary Fig. S7A**). To test this prediction, we performed co-immunoprecipitation assays from cells co-expressing Vps35^{yomCherry} and Gyp6^{V5} from their endogenous promoter. Both the wild-type and the catalytically dead variant Gyp6$^{R155A-V5}$ bound Retromer (**Figures 4I-4J**). However, Gyp6$^{\Delta PL-V5}$ (lacking PL motif residues 105-122) and Gyp6$^{\Delta C-V5}$ (lacking the C-terminal helix residues 415-458) both showed reduced binding efficiency. Simultaneous ablation of both predicted binding sites nearly abolished Retromer binding (**Figures 4I-4J**). Overall, our data suggest that two regions of Gyp6 mediate its interaction with Retromer, one around the PL motif and the other at the C-terminal tail, where the interactions involving the C-terminal tail can vary among Gyp6 homologues.

Gyp6 GAP activity and its binding to Retromer are required for Vps10 recycling

To examine the importance of yeast Gyp6 binding and activity for Retromer function *in vivo* we ablated or mutated the primary PL motif (Δ107-120 or R108G, L109G, T110R, V112G, P119G, L120A) and the C-terminal helix of Gyp6 (Δ415-458) and generated catalytically dead *gyp6^{R155A}* (Haas *et al*, 2005). The variants were C-terminally tagged with V5 and expressed from the endogenous Gyp6 promoter in the sensitized *gyp6Δ gyp3Δ ypt7^{Q68L}* background.

gyp6Δ gyp3Δ ypt7^{Q68L} cells accumulated Vps10^{mNG} on vacuoles as previously shown (**Figure 5A**). While wild-type GYP6 partially rescued this phenotype, catalytically inactive *gyp6*^{R155A} and the variant lacking the C-terminal helix in combination with PL motif did not (**Figure 5B**). In line with this mislocalization of Vps10, which is a sorting receptor for the vacuolar hydrolase CPY (Cooper & Stevens, 1996), all three *gyp6* mutants secreted CPY into the extracellular space around yeast colonies on an agar plate, which was not the case for wild-type cells (**Figure 5C**). Thus, both Gyp6 GAP activity and its binding to Retromer are required to support Retromer function in Vps10 retrieval and vacuolar protein sorting.

Ypt7 inactivation by GAPs promotes carrier departure

Cargo retrieval requires cargo capture in sorting domains and cargo transfer into tubulovesicular structures, which then detach to form cargo carriers. Failure of Retromer-dependent transfer of Vps10 from endosomes to the Golgi leads to the accumulation of Vps10 in the vacuolar membrane (Suzuki *et al*, 2019). If this failure is generated by a complete inactivation of the sorting machinery, such as by deleting Retromer, the accumulating cargo is homogeneously distributed over the vacuolar membrane (see **Figure 2A**). The situation is different when cargo collection remains functional, but cargo exit from the compartment is limiting, e.g., due to an overload of the sorting machinery by an excess of cargo. In this case, Vps10 concentrates in small, Retromer-containing zones from which tubular structures are formed and depart (Arlt *et al*, 2015).

To differentiate which of these processes might require Gyp6 GAP activity and Ypt7 inactivation, we examined whether the GAP mutants accumulated Vps10^{mNG} cargo in dot-like structures at the vacuolar membrane (**Figure 5A; Figure 6A**). If these zones correspond to Retromer-dependent cargo sorting domains, Vps35^{mCherry} should co-accumulate in the same structures. In line with this, *gyp6Δgyp3Δ* mutants showed larger and more intense Vps35^{yomCherry} clusters at vacuoles than wild-type cells. These Vps35 dots accumulated not only Vps10^{mNG} (**Figure 6A**) but also Ypt7 (**Figure 6B**). In *gyp6Δ gyp3Δ ypt7*^{Q68L} cells, vacuolar regions concentrating Vps10, Vps35 and Ypt7 were even more prominent (**Figure 6A-6B**). Importantly, they often displayed elongated or tubular shapes that accumulate both coat components (Vps35 ^{yomCherry}) and cargo (Vps10 ^{mNG}). Such structures were never observed in wild-type cells. These tubular structures resemble the tubulo-vesicular vacuolar Vps10 exit zones that can be

observed upon transient overexpression of Vps10, a treatment that overloads the endosomal retrieval system, generates a spill-over of Vps10 into the vacuolar membrane, and therefore triggers compensatory retrieval of the Vps10 from the vacuolar surface (Arlt *et al*, 2015). The vacuolar tubules in *gyp6Δ gyp3Δ ypt7*^{Q68L} cells can hence be considered as bona fide nascent cargo carriers.

To assay whether cargo-coat complexes indeed accumulate, we performed immunoprecipitations from *gyp6Δgyp3Δypt7*^{Q68L} cells co-expressing Vps35^{yomCherry} and Vps10^{mNG}. These cells showed two- to threefold more Vps10^{mNG} and Ypt7 associated with Vps35^{yomCherry} relative to wildtype cells (**Figure 7A**). Expression of wild-type Gyp6^{V5} in these cells attenuated this phenotype. Gyp6 variants that were catalytically dead (R155A) or lacking the PL motif and the C-terminal helix did not correct the accumulating coat-cargo-Ypt7 interactions (**Figures 7A and 7B**). Thus, Retromer-cargo complexes accumulate in the absence of Gyp6 activity or in the absence of Gyp6 recruitment to the coat.
In summary, this suggests that cargo collection and carrier formation by the coat can proceed with active, GTP-loaded Ypt7, but that GTP hydrolysis might be necessary to detach the carrier from the donor membrane. Ypt7 inactivation by GAP activity might then switch Retromer sorting domains from cargo collection to the departure of a carrier.

Discussion

RAB7 and its yeast homolog Ypt7 function in multiple trafficking pathways and interact with distinct sets of effectors, including tethering factors like the HOPS complex, cargo-sorting complexes such as Retromer, vacuole-mitochondria contact sites, and machinery involved in fusion of vacuoles with endosomes, autophagosomes, or with themselves (Seals *et al*, 2000; Liu *et al*, 2012; Wichmann *et al*, 1992; Hönscher *et al*, 2014; Cabrera *et al*, 2009; Elbaz-Alon *et al*, 2014). Given this functional diversity, we presume that RAB7 and Ypt7 are regulated by multiple GAPs that act in a context-dependent manner to ensure spatial and temporal precision of their inactivation, tailored to the respective function. Our findings provide new insights into the coordination of Ypt7 inactivation and Retromer-mediated cargo sorting, highlighting a role for the GAP protein Gyp6 in coupling GTP hydrolysis with carrier formation. While Retromer has been extensively studied in the context of cargo recognition and membrane remodeling (Harrison *et al*, 2014; Courtellemont *et al*, 2022; Kovtun *et al*, 2018; Cui *et al*, 2018), its regulation by Rab GAPs is relatively poorly understood. Here, we propose that yeast Gyp6 functions as a spatiotemporal regulator of Retromer activity by acting as a Ypt7 GAP during cargo recycling.

GAPs can be promiscuous *in vitro* and, perhaps for this reason, show redundancy in the *in vivo* situation (Lamber *et al*, 2019). This renders the assignment of a GAP to a specific RAB GTPase challenging. Our interaction analyses support an interaction of Gyp6 with Ypt7 in the context of endosomal protein sorting, where both proteins are brought into proximity through their common interaction with Retromer. In line with this, *gyp6Δ* mutants had the strongest impact on endosomal protein sorting by Retromer. Gyp7, a well-characterized Ypt7 GAP that regulates fusion at endosomes and vacuoles (Brett *et al*, 2008; Vollmer *et al*, 1999; Albert *et al*, 1999; Füllbrunn *et al*, 2024), showed no impact on Retromer-dependent Vps10 sorting and only weak signals in the Retromer interaction screen. Gyp3 has a significant effect on Retromer cargo sorting, although its TBC domain showed much weaker GAP activity with Ypt7 than that of Gyp6, in agreement with previous results (Lachmann *et al*, 2012; Albert & Gallwitz, 1999). Since Gyp3 has a well-described role as a GAP for the Rab5 orthologue Vps21 (Lachmann *et al*, 2012; Nickerson *et al*, 2012), it may impact Retromer-dependent sorting indirectly through its influence on endosomal RAB-GTPase conversion. For example, Gyp3 deletion could result

in hyperactivation of Vps21 and, consequently, enhanced recruitment of the Ypt7-GEF (Mon1–Ccz1 complex), Ypt7 hyperactivation, activation of endosome-vacuole fusion and a resulting missorting of Vps10 to endosomes (Lachmann *et al*, 2012). This could also explain the additive effect of *gyp3Δ* and ypt7^{Q68L} on Retromer-dependent sorting. While our results do not exclude a function of Gyp3 on Retromer-associated Ypt7, our structural analysis and the presence of dedicated Retromer binding motifs lead us to propose Gyp6 as the genuine GAP of Ypt7 in the context of Retromer.

Our data support the view that Ypt7^{Q68L}, which is generally presumed to represent a constitutively active form, remains partly functional *in vivo* (Vollmer *et al*, 1999) and that its GTPase activity can be substantially stimulated by GAP proteins to inactivate its effector function on Retromer, albeit at a slower rate. Combining the *ypt7^{Q68L}* allele with *gyp3Δ* and *gyp6Δ* leads to the accumulation of Vps10 cargo in clusters at or near the vacuolar membrane that are enriched for both Retromer and Ypt7, and to the accumulation of Retromer complexes with both cargo and Ypt7. Impairing Ypt7 GTP hydrolysis in this way also leads to the accumulation of extended tubules that carry cargo and Retromer, suggesting that while tubule initiation can occur, carrier detachment may require RAB inactivation. This observation supports a model in which Ypt7-GTP promotes cargo clustering and carrier assembly, but its timely inactivation by Gyp6 is necessary for membrane remodeling and carrier release.

While Ypt7 can directly interact with Retromer, the Vps5 – Vps17 SNX-BARs can in turn displace Ypt7 from Retromer (Purushothaman *et al*, 2017; Liu *et al*, 2012; Balderhaar *et al*, 2010). Our previous study also demonstrated that Retromer forms a tight pentameric complex with Vps5 and Vps17 on the membrane via a PL motif in Vps5, which also binds to Vps29 (Chen *et al*, 2025). The Gyp6 PL motif has a lower binding affinity for Vps29 compared to that of Vps5. A stable Gyp6-Retromer complex is hence formed only when the PL motif and the C-terminal tail of Gyp6 are engaged simultaneously. In this conformation, the arginine finger essential for Rab GTP hydrolysis is positioned adjacent to the PL motif – Vps29 interface, far from Ypt7, which is predicted to reside near the N-terminal region of Vps35 (Harrison *et al*, 2014; Gonzalez-Lozano *et al*, 2025). Thus, Gyp6-mediated inactivation of Ypt7 requires a conformational change or dissociation from Retromer. We speculate that Vps5, which binds Retromer with a high affinity, could outcompete the Gyp6 interaction. In this scenario, Gyp6

may remain weakly bound to Retromer through its C-terminal tail, forming a more flexible complex. While Gyp6 remains bound to Retromer, it may inactivate nearby Ypt7 and thereby favor Ypt7 dissociation from Retromer and the formation of the competing Retromer-SNX-BAR complex. This hypothesis is supported by our data, which show that additional deletion of the C-terminal helix of Gyp6 causes a more pronounced defect in Vps10 sorting than deletion of the PL motif alone. A complete sorting defect is observed only when both the PL motif and the C-terminal binding helix are deleted, highlighting the importance of both regions. Given that Gyp6 could be displaced by Vps5 at the PL motif site, we envision a handover mechanism to regulate GAP activity through the assembly of the pentameric Retromer-SNX-BAR complex. Combining our data with the published observations mentioned above, we propose the following model: (1) Active Ypt7 recruits the Retromer to endosomes; (2) With increasing Retromer density, Gyp6 is recruited; (3) Retromer binds cargo such as Vps10 in conjunction with adaptors such as Vps5-Vps17 sorting nexins that bind Retromer through their PL motifs (4); these competing PL motifs liberate Gyp6 to inactivate Ypt7; (6) GTP hydrolysis facilitates membrane fission and carrier release. The catalytic role of Gyp6 and its ability to interact with Retromer thus suggest a mechanism for a Rab-GTPase-controlled switch from coat assembly and cargo collection to carrier release. Given the similarity between Gyp6 and the metazoan GAP TBC1D5 (Jia *et al*, 2016) in their mode of interacting with Vps29 through their PL motifs we assume that this spatiotemporal regulation of carrier formation through GAP handover and Rab-GTPase switching is a general feature of Retromer.

Materials and Methods

Yeast Strains and Genetic Manipulations

S. cerevisiae strains used in this study are listed in **Table S3**. Genetic manipulations were made using the CRISPR-Cas9 approach and confirmed by PCR and sequencing. The plasmids used to carry out CRISPR-Cas9 genome editing were obtained by cloning hybridized oligonucleotides coding for the sgRNA between the XbaI and AatII restriction sites of the parent plasmid (pSP473, pSP474, pSP475, or pSP476, **Table S4**). The oligonucleotides used for hybridization and to control strains by PCR or sequencing are listed in **Table S5**. The integrative plasmids used in this study are listed in **Table S4**. Cells were cultured for transformation at 30°C to mid-log phase in YPD medium (1% [wt/vol] yeast extract, 2% [wt/vol] Bacto Peptone, and 2% [vol/vol] glucose) or with YNB medium (0.17% [wt/vol] yeast nitrogen base without amino acids and ammonium sulfate, 0.5% [wt/vol] ammonium sulfate, and 2% [vol/vol] glucose) supplemented with the necessary amino acids.

Proximity labelling

Purification of biotinylated proteins via streptavidin beads

Method adapted from (Cho *et al*, 2020). Cells expressing TurboID-V5-Ypt7, *ypt7*^{Q68L} or *ypt7*^{T22N} (in a BJ3505 *ypt7Δ* background) and TurboID-V5 (in BJ3505 wild-type background) were grown overnight in SC-URA to an OD_{600} of 0.3 (~ 0.6×10^7 cells). From a freshly prepared biotin stock (100 mM) in dimethyl sulfoxide (DMSO), 100 µM was added to cultures, and cells were grown for another 3 h to a final OD_{600} of 0.8–1. Around 350-400 OD_{600} equivalent units of cells were harvested by centrifugation at 3000 rpm for 10 min, washed twice with ddH_2O, and cell pellet resuspended in RIPA lysis buffer (50 mM Tris, 150 mM NaCl, 0.1% SDS, 0.5% sodium deoxycholate, 1% Triton X-100, 1x PIC, 1 mM PMSF). Whole-cell lysates were obtained using French Press in RIPA lysis buffer. Free biotin was depleted from the cell extract using Zeba Spin Desalting Columns 7K (Thermo Scientific™ Zeba™ Spin Desalting Columns). Clarified lysates containing around 2.5 mg protein per sample were incubated overnight in 100 µL of pre-equilibrated streptavidin magnetic beads with RIPA buffer (Pierce™ Streptavidin Magnetic Beads, Thermofisher) at 4°C with rotation.

Magnetic beads were subsequently washed in the following order: RIPA buffer (2 min @RT, twice), 1 M KCl (2 min @RT), 0.1 M Na_2CO_3 (10 sec @RT), 2 M Urea in 10 mM Tris-HCl pH 8.0 (10 sec @RT) and RIPA buffer (2 min @RT, twice). The beads were then resuspended in fresh RIPA lysis buffer, transferred to a new Eppendorf tube, the buffer was removed, and the dry beads were sent to the Protein Analysis Facility (UNIL) on dry ice for further processing and preparation for LC-MS/MS analysis. For control purposes, 5% of beads were eluted with 4x-Nupage (Thermofisher) supplemented with 2 mM Biotin and 20 mM DTT and boiled for 10 min at 95°C (Vf= 30 µL). 10 µL of eluted sample was loaded into 10% SDS-PAGE gel followed by overnight WB transfer. The Streptavidin-IRDye 680 was used to visualize biotinylated proteins.

Proteomics analyses

All raw MS data together with raw output tables are available via the Proteomexchange data repository (www.proteomexchange.org) with the accession PXD073331.

Protein digestion

Samples were digested following a modified version of the iST method (Kulak *et al*, 2014) (named miST method). 25 µL of miST lysis buffer (1% Sodium deoxycholate, 100mM Tris pH 8.6, 10 mM DTT), were added to the beads. After mixing and dilution 1:1 (v:v) with H_2O, samples were heated 10 min at 75°C. Turbo-ID beads were first digested with 0.5 µg of trypsin/LysC mix (Promega #V5073) for 1h at 25°C, and sample supernatants were transferred to new tubes. Beads were washed with 50 µL of miST buffer diluted 1/1 in H_2O, and supernatants were pooled with the previous ones. Reduced disulfides were alkylated by adding 25 µL of 160 mM chloroacetamide (32 mM final) and incubating for 45 min at 25°C in the dark. Samples were then digested overnight at 25°C with 1.0 µg trypsin/LysC mix.

To remove sodium deoxycholate after digestion, two sample volumes of isopropanol containing 1% TFA were added to the digests, and the samples were desalted on a strong cation exchange (SCX) plate (Oasis MCX; Waters Corp., Milford, MA) by centrifugation. After washing with isopropanol/1%TFA, peptides were eluted in 200ul of either 80% MeCN, 19% water, 1% (v/v) ammonia and dried by centrifugal evaporation.

Liquid Chromatography-Mass Spectrometry analyses

Data-dependent LC-MS/MS analyses of samples were carried out on a Fusion Tribrid Orbitrap mass spectrometer (Thermo Fisher Scientific) interfaced through a nano-electrospray ion source to an Ultimate 3000 RSLCnano HPLC system (Dionex), via a FAIMS interface. Peptides were separated on a reversed-phase custom packed 45 cm C18 column (75 µm ID, 100Å, Reprosil Pur 1.9 µm particles, Dr. Maisch, Germany) with a 4-90% acetonitrile gradient in 0.1% formic acid at a flow rate of 250 nl/min (total time 140 min). The MS acquisition method used cycled through three compensation voltages (-40, -50, -60V) to acquire full MS survey scans at 120'000 resolution. A data-dependent acquisition method controlled by Xcalibur software (Thermo Fisher Scientific) was set up that optimized the number of precursors selected ("top speed") of charge 2+ to 5+ from each survey scan, while maintaining a fixed scan cycle of 1.0 s per FAIMS CV. Peptides were fragmented by higher energy collision dissociation (HCD) with a normalized energy of 32%. The precursor isolation window used was 1.6 Th, and the MS2 scans were done in the ion trap. The *m/z* of fragmented precursors was then dynamically excluded from selection during 60 s.

Data processing

Data files were analysed with MaxQuant 2.4.7 (Cox & Mann, 2008) , incorporating the Andromeda search engine (Cox *et al*, 2011) . Cysteine carbamidomethylation was selected as a fixed modification while methionine oxidation and protein N-terminal acetylation were specified as variable modifications. The sequence databases used for searching were the yeast (*Saccharomyces cerevisiae*) reference proteome based on the UniProt database (www.uniprot.org, version of March 1st, 2023, containing 6'060 sequences), and a "contaminant" database containing the most usual environmental contaminants and enzymes used for digestion (keratins, trypsin, etc). Mass tolerance was 4.5 ppm on precursors (after recalibration) and 0.5 Da on MS/MS fragments. Both peptide and protein identifications were filtered at 1% FDR relative to hits against a decoy database built by reversing protein sequences.

Data analysis

All subsequent analyses were done with an in-house developed software tool (available on https://github.com/UNIL-PAF/taram-backend). Contaminant proteins were removed, and

intensity iBAQ values (Schwanhausser *et al*, 2011) were log2-transformed. After assignment to groups, only proteins quantified in at least 4 samples of one group were kept. Missing values were imputed based on a normal distribution with a width of 0.3 standard deviations (SD), down-shifted by 1.8 SD relative to the median. Student's T-tests were carried out among conditions, with Benjamini-Hochberg correction for multiple testing (adjusted p-value threshold <0.05). Imputed values were later removed. The difference of means obtained from the t-tests were used for 1D enrichment analysis on associated GO/KEGG annotations as described (Cox & Mann, 2012) . The enrichment analysis was also FDR-filtered (Benjamini-Hochberg, adjusted p-value <0.02). The -log10 of the adjusted p-value was calculated, and the graphs were generated using GraphPad PRISM software 10.4.0.

FM 4-64 staining and confocal microscopy

Cells were inoculated from a pre-culture in stationary phase and grown overnight to early mid-logarithmic phase (OD_{600} 0.5 - 0.8) at 30°C, 200 r.p.m. After dilution to an OD_{600} of 0.2 - 0.3 in 1 mL of fresh medium, FM 4-64 (N-(3-triethylammoniumpropyl)-4-(6-(4-(diethylamino) phenyl) hexatrienyl) pyridinium dibromide) in DMSO was added to a final concentration of 10 µM. Cells were stained for 60 min, followed by two washing steps in medium without dye (centrifugation at 3,000 rpm for 2 min) and a subsequent chase of 90 - 120 min (depending on the endocytic capacity of the strain) in 1 mL of fresh medium.

Imaging was performed with a NIKON Ti2 spinning disc confocal microscope with a 100×1.49 NA lens. Imaging was done at room temperature in YNB medium using GFP and mCherry channels with different exposure times according to the fluorescence intensity of each protein. Z-stacks were obtained with a spacing of 0.2 µm between each single focal plane and assembled, when required, into average projections containing five single slices around the middle of the cell. All experiments were repeated at least three times.

To investigate the function of the Retromer, the localization of vacuolar $Vps10^{mNG}$ in different strains was assessed from at least 150 cells per experiment across three independent biological replicates. Mean, SEM calculations from stacks containing around 150 - 200 cells per strain were done in Excel and plots were obtained with GraphPad PRISM software.

Total cell extracts by TCA

To prepare cell lysates, cells were grown overnight to mid-log phase (OD_{600} 0.5 - 1) at 30 °C from a saturated pre-culture. 2 OD units of cells were harvested by centrifugation (3000 rpm, 3 min). The obtained cell pellet was resuspended in 200 µL of 20% trichloroacetic acid (TCA) and lysed by bead beating with glass beads (0,25 - 0,5 mm, Carl Roth) for 15 min at 4°C using a VIBRAX (IKA). After lysis, 400 µL of 40% TCA was added, supernatant collected and centrifuged at 14,000 rpm for 10 min at RT. Cell lysates were solubilized in 4x-Nupage (containing 1 M Tris and 5% β-mercaptoethanol) at 98°C for 10 min and centrifuged (14,000 rpm, 2 min, RT) to remove cell debris. Equal amounts (0.5 - 0.75 OD_{600} equivalents of cells per sample) were analyzed by Western blot using anti-Ypt7 (homemade), anti-mNeonGreen (32f6-100, Chromotek), anti-mCherry (ab125096, Abcam), anti-V5 (460705, Novex), anti-G6PDH (A9521-1VL, Sigma), anti-Pgk1 (ab113687, Abcam). Detection was carried out using IRDye 680 or 800RD-conjugated secondary antibodies.

CPY sorting assay

Yeast strains were cultured overnight to achieve saturation in the appropriate medium at 30°C. A 2 µL aliquot of each saturated culture was applied onto YPD agar plates and incubated at 30 °C for 16 hours. Following this, the colonies were covered with nitrocellulose membranes and incubated overnight at 30°C. The membranes were subsequently rinsed with double-distilled water (ddH_2O) and incubated for 1 hour in TBST buffer containing 5% non-fat milk to block nonspecific binding. The membrane was probed for the secreted protein carboxypeptidase Y (CPY) using an anti-CPY mouse monoclonal antibody (ab113685; Abcam) for 4 hours at room temperature. Detection was carried out using an IRDye 800RD-conjugated goat anti-mouse secondary antibody (926-32210; LI-COR).

Immunoprecipitation

The interaction between cargo (Vps10), Retromer, and Ypt7 was analyzed following a protocol adapted from the study (Suzuki *et al*, 2019). Briefly, cells expressing $Vps10^{mNG}$ and $Vps35^{yomCherry}$, from their endogenous promoter, were cultured overnight until they reached the mid-logarithmic phase (OD_{600} between 0.8 and 1.0), starting from a saturated pre-culture.

A total of 50 mL of cells were collected, washed twice with immunoprecipitation (IP) buffer (20 mM Hepes-KOH, pH 7.2, 0.2 M sorbitol, 50 mM AcOK, 1 x protease inhibitor cocktail, 1 mM PMSF), and then harvested. The cells were lysed with 0.5-mm zirconia beads in 250 µL of IP buffer for 5 minutes at 4°C using a VIBRAX (IKA). To this lysate, 250 µL of IP buffer containing 2.0% saponin was added, to obtain a final concentration of 1.0%. The samples were then rotated at 4°C for 60 minutes at 10 rpm. The solubilized lysates were clarified by centrifugation at 500 g for 5 minutes at 4°C, followed by high-speed centrifugation at 17,500 g for 10 minutes. The resulting supernatants were normalized to 10 mg of total protein per sample, measured by Nanodrop, and incubated with pre-equilibrated anti-RFP magnetic agarose beads (RFP-Trap Magnetic Agarose from Chromotek) at 4°C for 3 h. After incubation, the beads were washed three times with IP buffer containing 1.0 % saponin. Before the final washing step with IP buffer, beads were transferred into a new Eppendorf tube. The bound proteins were eluted by heating the beads in 4 x Nupage buffer (containing 5% β-mercaptoethanol, 10 mM DTT, 1 mM PMSF, and 1 x protease inhibitor cocktail) at 95°C for 10 minutes. Samples were loaded into a freshly prepared SDS-PAGE gradient gel (4-18%).

To evaluate the interaction between Retromer and Gyp6, a co-immunoprecipitation protocol adapted from the previously described method was employed with minor modifications. Yeast cells expressing Gyp6^{V5} (or its variants) and Vps35^{yomCherry}, under endogenous promoter, were cultured overnight from saturated pre-cultures and harvested at mid-log phase (OD_{600} = 0.8–1.0). A total of 75 mL of culture was collected, washed twice with TGN buffer (50 mM Tris-HCl, pH 7.4, 100 mM NaCl, 5% [v/v] glycerol, 1x protease inhibitor cocktail, 1 mM PMSF), and pelleted by centrifugation. Cell lysis was performed at 4℃ using 0.5-mm zirconia beads in 300 µL of TGN buffer for 5 minutes using a VIBRAX (IKA). Subsequently, 300 µL of TGN buffer containing 1.0% Triton X-100 was added to the lysate to achieve a final detergent concentration of 0.5%. Samples were rotated at 4°C for 60 minutes at 10 rpm to facilitate membrane solubilization.

The lysates were clarified by centrifugation at 500 x g for 5 minutes at 4℃, followed by a second centrifugation step at 17,500 x g for 10 minutes. The resulting supernatants were adjusted to a final protein concentration of 10 mg in a total volume of 500 µL (quantified via NanoDrop) and incubated with pre-equilibrated anti-RFP magnetic beads (RFP-Trap Magnetic

Particles, Chromotek) for 2 hours at 4°C. Following incubation, beads were washed three times with TGN buffer containing 0.5% Triton X-100. Before the final wash with detergent-free TGN buffer, the beads were transferred to fresh microcentrifuge tubes. Bound proteins were eluted by incubating the beads in 4× NuPAGE sample buffer (supplemented with 5% β-mercaptoethanol, 10 mM DTT, 2 mM PMSF, and 1 × protease inhibitor cocktail) at 95°C for 10 minutes. Eluted proteins were resolved by SDS-PAGE using freshly cast 4–18% polyacrylamide gradient gels.

Western blot

All Western blot analysed in this study were performed using a LI-COR Odyssey SA system to detect secondary antibodies conjugated with fluorescent labels. The intensities of the corresponding bands were quantified using FIJI software. All measurements were carried out across a minimum of three independent experiments, as described in the figure legends. All the calculations were done in Excel, and graphs were generated using Prism 10.4.0.

Molecular biology and cloning for bacteria expression

cDNA encoding full-length ctVps29 (uniport number: G0RZB5), ctVps26 (uniport number: G0S0E6) and ctVps35 (uniport number: G0S709) were cloned into pET28a and pGEX6P1 vectors similar to the one described previously (Chen *et al*, 2025). ctVps29 for the ctGyp6L (no uniport number, GenBank: KAH6850218.1) binding experiment was also cloned into pET28a vector but with an uncleavable C-terminal His6-tag. All the GAP and Ypt7 constructs in this study including ctGyp3^{TBC}/ctMsb3^{TBC} (uniport number: G0S722), ctGyp6L^{TBC} (residues 1 to 374), LsmA-ctGyp6L$^{676-773}$, ctGyp7^{TBC} (uniport number: G0SFD4), Gyp6, ctYpt7 (uniport number: G0SGE1), ctVps21 (uniport number: G0SHN0), ctRab5like (uniport number: G0SHY4) and Ypt7 were cloned into pGEX6P1 vector. For ctYpt7, ctVps21, ctRab5like and Ypt7, the C-terminal Cys, Ser and Cys were substituted with His$_6$-tag to mimic the prenylation. Site-directed mutagenesis was performed to generate mutant constructs with custom-designed primers. All constructs were verified using DNA sequencing.

Recombinant protein expression and purification in bacteria

All the bacterial constructs including ctRetromer, ctGyp3^{TBC}, ctGyp6L^{TBC}, ctGyp7^{TBC}, ctYpt7, ctVps21, ctRab5like, LsmA-ctGyp6L$^{676-773}$, Gyp6, Ypt7 and associated mutants were expressed in BL21 (DE3) competent cells using autoinduction method as described previously (Chen *et al*, 2025). To produce ctRetromer trimer complex, GST-tagged ctVps29 and untagged ctVps35 co-expressed cell pellet were mixed with N-terminal His-tagged ctVps26 and resuspended in lysis buffer containing 50 mM Tris-HCl pH 7.5, 200 mM NaCl, 50 µg/ml benzamidine and DNase I before passed through a Constant System TS-Series cell disruptor. To generate ctRetromer specifically for ctGyp6^{TBC} binding experiment, C-terminal His$_6$-tagged ctVps29 and GST-tagged ctVps35 co-expressed cell pellet were used. As we found the GST and the PreScisison protease recognition site on the N-terminus of ctVps29 likely affect ctGyp6 from binding. For all constructs, the lysate was clarified by centrifugation and the supernatant was loaded onto either Talon® resin (Clontech) or glutathione Sepharose (GE healthcare) for initial purification. For ctRetromer, both Talon® resin (Clontech) and glutathione Sepharose (GE healthcare) were applied to obtain the correct stoichiometry ratio of the complex. On-column PreScission protease cleavage of GST tag was performed overnight at 4°C using protocol described previously (Chen *et al*, 2025). The flow-through containing the fusion tag cleaved protein was further purified using size-exclusion chromatography (SEC) using either HiLoad® Superdex 200 or Superdex 75 16/600 columns equilibrated with a buffer containing 50 mM Tris-HCl pH 7.5, 200 mM NaCl, 2 mM β-ME.

To obtain the active and inactive form of Ypt7 constructs, the purified wild-type ctYpt7 and Ypt7 in SEC buffer were treated with 1 mM EDTA and 1 mM DTT. After 1 hour incubation on ice, 1.5 mM of either non-hydrolyzable GTP analog GppCp (Abcam) or GDP was added to the sample together with 10 mM $MgCl_2$ and incubated on ice for further 1 hour. The reaction was terminated by passing the sample mixture onto an analytical Superdex 75 10/300 increase column using the SEC buffer described above.

Crystallization and data collection

All crystals were grown by hanging-drop vapor diffusion method at 20°C. Diffraction quality crystal of ctGyp6L^{TBC} was obtained using a protein concentration of 12 mg/ml in condition

composed of 0.1 M Bis-Tris pH 6.5, 25% PEG 3350 and 5% glycerol. For the co-crystallization, 3 molar excesses of ctGyp6L$^{87-107}$ peptide or Gyp6$^{105-122}$ peptide was added to the purified mVPS29 at a final concentration of 11 mg/ml. Diffraction crystal of mVPS29 – ctGyp6L$^{87-107}$ peptide was obtained in condition containing 0.2 M sodium fluoride, 18% PEG 3350 and 5% glycerol. For the mVPS29 – Gyp6$^{105-122}$ peptide crystals, the best condition composed of 0.1 M Tris-Base pH 8.5, 22% PEG 3350. Crystals grew after 14 days were directly cryoprotected in reservoir solution except for the Gyp6 peptide containing crystals where an additional 5% glycerol were added. X-ray diffraction data were carried out at the Australian Synchrotron MX2 beamline at 100 K.

Structure determination

The data collected were indexed and integrated using AutoXDS and scaled using Aimless (Evans & Murshudov, 2013; Kabsch, 2010). Both structures were solved by molecular replacement (MR) using Phaser (Mccoy *et al*, 2007). In the case of ctGyp6L TBC domain crystal, a model generated by Alphafold2 were applied as the template. For the Gyp6 peptide containing crystal structures, the wild-type human VPS29 structure (PDB ID: 6XS7) was used as the template. The initial electron density map obtained after MR guided the locations of the mVPS29, ctGyp6L TBC domain and the peptides. Structure refinement was performed with PHENIX beginning with rigid-body refinement (Adams *et al*, 2010), Translation-Libration-Screw (TLS) and isotropic B factors. The program Coot was used to inspect and fitting of resulting model guided by Fo–Fc difference maps. Ordered water molecules were first automatically included in the model, followed by manual inspection. The coordinates for small ligands such as glycerol, PEG and β-ME were generated using LIBCHECK from Coot. Molprobabity was used to evaluate the quality and geometry of the refined structures (Williams *et al*, 2018). Data collection and refinement statistics are summarized in **Table S2**. Molecular figures were generated using PyMOL and structural comparison was performed using FALI and Foldseek (Kempen *et al*, 2023). Sequence conservation was mapped on the structure with ConSurf server (Ashkenazy *et al*, 2016).

Isothermal Titration Calorimetry

ITC experiments on ctVps29 and Gyp6 interactions were performed using a Microcal PEAQ ITC (Malvern) at 30°C. All the proteins and peptides including ctVps29, ctGyp6L$^{87-107}$, ctGyp6L^{TBC} and Gyp6$^{105-122}$, used for ITC experiments were prepared in buffer containing 50 mM Tris-HCl pH 7.5, 200 mM NaCl, 2 mM β-ME. To confirm the binding of Gyp6 PL motif is required for binding to Retromer, 350 µM of Gyp6$^{105-122}$ was titrated into 13 µM of ctVps29. In the case of ctGyp6 and ctRetromer binding experiment, 1000 µM of ctGyp6L^{TBC} was titrated into 40 µM of ctVps29. The effect of cyclic peptides on blocking the PL motif-mediated binding was carried out by adding 5 molar excess RT-D3 into ctVps29 prior of the titrating experiments. To investigate the binding between ctGyp6L tail and ctRetromer, 400 µM - 600 µM of ctGyp6L$^{680-698}$ or ctGyp6L$^{760-773}$ peptides were titrated into 14 µM of ctRetromer. The binding experiment using chimera construct was done by titrating 580 µM of either wild-type or IL/F mutant of LsmA-ctGyp6L$^{676-773}$ into 13 µM of ctRetromer. In all cases, the ITC experiments were performed with a single injection of 0.4 µl (not used in data processing) followed by 12 series injections of 3.22 µl each, spaced 180 sec intervals and stirred at 750 rpm. The thermodynamic parameters of binding including the dissociation constants (Kd,), enthalpy (ΔH), and Gibbs free energy (ΔG) were obtained after fitting the integrated and normalized data to a single-site binding model. The stoichiometry (N) was refined initially, and the if the value obtained was close to 1, then, N was set to exactly 1.0 for calculation. Data presented are the mean of triplicate titration for each experiment.

AlphaFold Predictions

All protein models displayed in the manuscript were generated using either AlphaFold2 Multimer implemented in the Colabfold interface (Mirdita *et al*, 2022) or AlphaFold3 server (https://alphafoldserver.com/) available on the Google platform. The default settings for ColabFold were used to construct multiple sequence alignments using MMseqs2 (Mirdita *et al*, 2019). For all modelling experiments, we assessed (i) the prediction confidence measures (pLDDT and interfacial iPTM scores), (ii) the plots of the predicted alignment errors (PAE) and (iii) backbone alignments of the final structures. The screening of Ypt7 and the TurboID captured interactors was done using batch mode. The confidence level of scRetromer and Gyp proteins screening were calculated using the sum of IPTM score generated by AlphaFold3 and

AlphaFold2. For clarity, the confidence level score was differentiated into two groups as full-length scRetromer (as X-Y plot) and individual subunits (as heatmap). All the graphs were generated using Prism 10.4.0.

GTPase activity assay

GTPase activity was performed in the GTPase-GloTM assay (Promega) using manufacturer's instructions. In brief, 5 µl of protein/protein mixtures (in general, 1 to 2 µM of Ypts, 0.8 to 1 µM GAPs and 3 µM ctRetromer) was mixed with 5 µL of GTP-solution composed of 10 µM GTP, 1 mM DTT, 50 mM Tris-HCl pH 7.5, 100 mM NaCl, 10 mM $MgCl_2$ in 384-well plates. To initiate the GTP reaction, the reaction mixture was incubated for 70 to 80 min at 25°C. The reaction was terminated by adding 10 µL of GTP-Glo buffer, which contains a nucleoside-diphosphate kinase that converts remaining GTP in the solution to ATP. The measurement was carried out by adding 20 µL of detection reagent containing a luciferase/luciferin mixture, making the ATP luminescent. In every set of assay experiments, a GTP-solution buffer sample without protein was used as the control and for normalization (represented as 0% GTP hydrolysis). Reactions were carried out with at least 3 replicates per assay experiment to calculate the average and standard deviation. All the calculation was done in Excel, and graphs were generated using Prism 10.4.0.

Mass photometry

Molecular mass measurement of LsmA-ctGyp6L$^{676-773}$ was performed using a Refeyn OneMAP mass photometer (Refeyn Ltd) following manufacturer's instructions. In brief, the calibration was formed first using protein standards with known molecular weight (i.e., 66, 132 and 480 kDa) in buffer containing 50 mM Tris-HCl pH 7.5, 200 mM NaCl, 2 mM β-ME. Next, 3 µL of purified LsmA-ctGyp6L$^{676-773}$ at a final concentration of 50 nM – 100 nM was loaded onto the mass photometer, and 100 frames were recorded. The precise molecular mass was calculated using the calibration standards measured as reference.

Acknowledgements:

We thank the Protein Analysis Facility of the Faculty of Biology and Medicine, University of Lausanne, Lausanne, Switzerland, for mass spectrometry-based protein analytics. We acknowledge the use of the Protein Analysis facility of UNIL, of the University of Queensland

Centre for Microscopy and Microanalysis (CMM) Facility, and the assistance of K. A. Arachchige. X-ray data were collected on the MX2 beamline at the Australian Synchrotron. B.M.C. is supported by an Investigator Grant from the National Health and Medical Research Council (APP2016410). AM has been supported by grants from the SNSF (31003A_179306, 310030_204713, and 10.006.083).

Author contributions:

A.C.A., K.-E.C., B.M.C., and A.M. conceived the study. A.C.A., performed cell-based experiments and imaging. Protein preparation was performed by A.C.A., K.-E.C., Q.G, and S.E. K.-E.C., performed biochemical characterization, assays, protein crystallography, and structural analysis. K.-E.C., and M.H., performed in silico screening and modelling. M.L., performed peptide synthesis. A.C.A., K.-E.C., B.M.C., and A.M. supervised the research. Manuscript and figures were prepared by A.C.A., K.-E.C., B.M.C., and A.M.

Conflicts of Interest:

The authors declare that they have no conflict of interest.

Figure Legends

Figure 1: Identification of cognate GAPs of Ypt7 by proximity labelling.

(A) Volcano plot of TurboID-Ypt7 proximity labelling versus control cells expressing only cytosolic TurboID, from a proteomics analysis of streptavidin-biotin pulldowns. Selected relevant hits are indicated and marked with color. Gray dots correspond to selected non-significant hits (significance < 0.05). All interactors detected for each Ypt7 variant are provided in the supplementary datasheet XX. **(B)** The heatmap depicts the Fold Change (FC) value of all GAP proteins for each Ypt7 form (Wild-type, Q68L, and T22N). **(C)** Schematic diagram showing the number of targets identified from the TurboID-Ypt7 with an AF2 IPTM score ≥ 0.5. **(D)** Screening of potential Ypt7 direct interactors using AF2 and AF3. The confidence of interactors was assessed based on the sum of the interfacial PTM score (iPTM), averaged across three AF2 models, AF3 models and pDOCKQ score. From left to right, the list of Ypt7 interactors is ordered from high (0.85) to low (0.53) AF2 iPTM score, respectively. **(E)** List of TurboID targets showing a high confidence score with the ability to interact directly with Ypt7. **(F)** The PAE plots for the top-three ranked models of Ypt7 – Retromer complex predicted by AlphaFold2. **(G)** Cartoon representation of the top-ranked model Ypt7 – Retromer complex. The iPTM score represents the averaged iPTM score from the three models.

Figure 2: Vps10 recycling defect in GAP mutants.

(A) Live-cell fluorescence microscopy of yeast expressing Vps10^{mNeonGreen} (cyan) following FM 4-64 pulse-chase labelling to mark the vacuolar membrane (magenta). Representative z-stack average projections from 5 single-focal planes are shown. Scale bar, 5 µm. **(B)** Quantification of Vps10 colocalization with the vacuolar membrane marker FM 4-64, obtained from three independent experiments (n=50 cells per experiment were classified). Mean ± s.e.m. are shown. *P*-values were calculated by One-way ANOVA. **(C)** Western blot analysis of carboxypeptidase Y (CPY) secretion in the indicated yeast strains. **(D)** Heat map showing the *in silico* screening of scRetromer subunits with scRab GAPs using AF2 and AF3. The confidence score of potential interactors was assessed based on the sum of the iPTM score from three AF2, AF3 models. **(E)** GAP activity of GST-tagged Gyp6 towards Ypt7. **(F)** GTP hydrolysis of Ypt7 in the presence of indicated concentration of GST-Gyp6. **(G)** Comparison of the GAP activity assay of wild-type and mutant form of ctGyp6L^{TBC} towards ctYpt7. **(H)** GTP hydrolysis of ctYpt7

in the presence of indicated concentration of GAPs including ctGyp3^{TBC} (purple line), ctGyp6L^{TBC} (blue line) or ctGyp7^{TBC} (orange line).

Figure 3: Structural basis confirming the Retromer and Gyp6 association through the PL motif. (A) PAE plots showing the top-ranked AF2 models of Retromer - Gyp6 complex (left), the Vps35$^{1-403}$ – Vps26 – Gyp6 (middle) and VPS35$^{501-944}$ – Vps29 – Gyp6 subcomplexes (right). **(B)** Structural representation of the top-ranked model of the Retromer – Gyp6 complex. For clarity, Gyp6 is shown in ribbon. **(C)** Overlay of the three predicted models of Vps35$^{501-944}$ – Vps29 – Gyp6 complex. For clarity, only the key PL motif of Gyp6 involved in binding is shown. **(D)** Close-up view of the contact region between Vps29 and the PL motif of Gyp6. Models are coloured according to the pLDDT score. **(E, F)** Sequence alignment of yeast Gyp family proteins highlighting that the PL motif is uniquely present in Gyp6 and is conserved across Gyp6 orthologs. (**G**) ITC measurements of Gyp6$^{105-122}$ peptide (left) and ctGyp6L^{TBC} domain (right) binding to ctVps29, in the presence or absence of Vps29-binding cyclic peptide, RT-D3. ITC graphs show the integrated and normalized data with a 1 to 1 ratio binding ratio. **(H)** Crystal structure of the mVPS29 – Gyp6$^{105-122}$ complex, showing two molecules in the asymmetric unit. The dashed box indicates the electron density of the Gyp6$^{105-122}$ peptide, corresponding to a stimulated-annealing OMIT Fo-Fc map contoured at 3σ. **(I)** Superimposition of the mVPS29 – Gyp6$^{105-122}$ crystal structure (light teal) and the corresponding AF2 model (bright orange), highlighting the key binding residues (scGyp6 residues G105 to D122 shown in light purple). For clarity, the scVps29 disordered loop composed of P163 to S245 is not shown. **(J)** Crystal structure of the mVPS29 – ctGyp6L$^{87-107}$ complex, showing a single molecule in the asymmetric unit. The dashed box highlights the electron density of the ctGyp6L$^{87-107}$ peptide, as shown in (**H**). **(K)** Close-up view of the mVPS29 – ctGyp6L$^{87-107}$ crystal structure and **(L)** the corresponding AF2 model as shown in Figure (**I**). **(M)** Surface representation of the ctVps29 – ctGyp6L (left) and Vps29 – Gyp6 (right) complexes, illustrating the two distinct PL motif binding modes. ctGyp6L adopts a conformation more similar to TBC1D5 (highlighted in red) than to Gyp6.

Figure 4: Gyp6 has a second binding site with Retromer to enhance its affinity. (A) Prediction of the disordered C-terminal tail of ctGyp6L and Gyp6, highlighting their differences. Disorder region predictions were mapped using the D2P2 web server. **(B)** Structural representation of

the top-ranked ctRetromer – ctGyp6L model, showing the C-terminal tail of ctGyp6L binding to the rear surface of ctVps35. For clarity, ctRetromer is shown as surface and ctGyp6L as ribbon. **(C)** Sequence conservation mapped onto the ctVPS35 surface, illustrating that the LF motif of the ctGyp6L C-terminal tail (shown in ribbon) binds to ctRetromer. **(D)** Overlay of the ctGyp6L tail – ctVps35 and FAM21A LFa repeat 19 – VPS35 models, demonstrating the conservation of the LFa motifs binding model at the C-terminal end of Vps35. **(E, F)** ITC measurements of ctGyp6L$^{680-698}$, ctGyp6L$^{760-733}$ peptides, and LsmA-ctGyp6L$^{676-773}$ binding to ctRetromer. All ITC graphs show the integrated and normalized data fit with a 1 to 1 ratio binding ratio. **(G)** Representation of the top-ranked AF3 model of the Retromer – Gyp6 complex, with sequence conservation mapped onto the surface. The C-terminal helix of Gyp6 binds to the Vps26 – Vps35 interface. **(H)** Sequence alignment of the Gyp6 C-terminal tail helix across the *Saccharomycetes* class. Arrows indicate conserved residues potentially involved in binding. **(I)** Co-immunoprecipitation from *ypt7^{Q68L} gyp3Δ gyp6Δ S. cerevisiae* cells. Lysates from these cells expressing the indicated variants of Gyp6^{V5} and Vps35 with or without an mCherry tag were incubated with anti-mCherry beads. The adsorbed proteins were probed by SDS-PAGE and Western blotting with the indicated antibodies. Gyp6 variants: ΔC: lacking aa 415-458; ΔPL: lacking aa 107+120. Input lanes contain 1.5% of the total lysate. **(J)** Blots from three independent experiments from (I) were quantified on a Licor Odyssey fluorescence scanner. The ratio of co-immunoprecipitated Gyp6^{V5} over Vps35^{mCherry} was normalized and set to 1 for the Gyp6 wildtype. Data represent mean ± s.e.m. from n = 3 independent experiments. Statistical significance was determined using one-way Anova.

Figure 5: Gyp6 GAP activity and its binding to Retromer required for Vps10 recycling. (A) Live-cell fluorescence microscopy of yeast expressing Vps10^{mNeonGreen} (cyan) following FM 4-64 pulse-chase labelling to mark the vacuolar membrane (magenta). In Wild-type cells, Vps10 localizes to discrete puncta, largely non-overlapping with FM 4-64, consistent with its presence in late-Golgi and endosomal compartments, while it accumulates at the vacuole membrane in GAP mutants. Representative Z-stack images, from 5 single-focal planes, are shown. Scale bar, 5 µm. **(B)** Quantification of Vps10 colocalization with the vacuolar membrane marker FM 4-64, obtained from three independent experiments (n=50 cells per experiment were classified). Means and standard error of the mean are shown. *P*-values were calculated by One-way ANOVA. **(C)** Western blot analysis of carboxypeptidase Y (CPY)

secretion in the indicated yeast strains. In wild-type cells, CPY is retained intracellularly, whereas secretion of CPY into the medium is observed in GAP mutants.

Figure 6: Inhibiting GAP activity leads to membrane tubule accumulation. (A) Live cell fluorescence microscopy of yeast cells co-expressing Vps10^{mNG} and Vps35^{yomCherry}. Tubular structures that accumulate both cargo and Retromer are indicated by white arrows. Insets show the boxed areas at higher magnification. **(B)** Fluorescence microscopy of yeast cells co-expressing Vps35^{mNG} and Ypt7^{yomCherry}. White arrowheads point to Vps35^{mNG} puncta co-accumulating Ypt7^{yomCherry}. The yellow box and arrowhead indicate tubular structures that can be frequently observed in these mutants. Insets show the areas within the white boxes at higher magnification. Scale bars: 5 μm.

Figure 7: Vps10 cargo and Ypt7 show an increased Retromer association in Gyp6 GAP mutants. (A) Co-immunoprecipitation was performed from yeast cell lysates expressing Vps35^{yomCherry}, Vps10^{mNG} and Gyp6^{V5}. Immunoprecipitates were collected using anti-mCherry beads and probed by immunoblotting with anti-mNG, anti-V5, anti-Ypt7 and anti-mCherry antibodies. Significant increase of both cargo and Rab GTPase with Retromer in Gyp6 mutants. Representative results from at least three independent experiments are shown. Input fractions are shown to assess expression and specificity. (**B**) The amount of Vps10 and Ypt7 co-immunoprecipitated was quantified and normalized to the level of Vps35^{mCherry}. Data represent mean ± s.e.m. from n = 3 independent experiments. Statistical significance was determined using one-way ANOVA.

Supplementary Information

Suplementary Figure 1. TurboID-V5-Ypt7 protein quantification. (A) Western blot analysis of TurboID-V5-Ypt7 (wt, Q68L and T22N variants) expression in yeast cells. Whole-cell lysates were probed with anti-V5 and anti-Ypt7 antibodies to detect TurboID fusion proteins. Comparable expression levels were observed across samples, ensuring differences in biotinylated interactors reflect proximity and not variation in TurboID expression. PGK1 served as loading control. A representative blot from three independent experiments is shown. **(B)** Immunoblot of streptavidin precipitates, before and after the addition of biotin, from cells expressing TurboID-V5-Ypt7 and TurboID-V5-ypt7^{Q68L}. Volcano plots of **(C)** TurboID-ypt7^{T22N} and **(D)** of TurboID-ypt7^{Q68L} proximity labelling versus control cells expressing only cytosolic TurboID, from a proteomics analysis of streptavidin-biotin pulldowns.

Supplementary Figure 2. In silico screening identified direct interactors of Ypt7. In all cases. the top three ranked models are aligned and shown in ribbon. The models are coloured according the pLDDT confidence score. Panel on the top of the models shows the predicted alignment error (PAE) plots for the top-ranked prediction of the complex. The ipTM score represent the averaged iPTM score from the top three-ranked models. HOPS complex – Ypt7 model was generated by combining the prediction from multiple subcomplexes including Vps11 – Vps18 – Vps41$^{729-992}$ complex, Vps18$^{626-918}$ – Vps16 – Vps33 – Vps41$^{729-992}$ complex, Vps11$^{559-1029}$ – Vps18$^{1-658}$ – Vps39 – YPT7^{GTP} complex and Vps41 – Ypt7^{GTP} complex. All 4 models were combined using the previous CryoEM structure (PDB ID: 7ZU0) as the template.

Supplementary Figure 3: Effect of *gyp7Δ* mutations on Vps10-mNG localisation in the ypt7 Q68L background. Live-cell fluorescence microscopy of yeast expressing Vps10^{mNeonGreen} (cyan) following FM 4-64 pulse-chase labelling to mark the vacuolar membrane (magenta) as shown in Figure 2A.

Supplementary Figure 4: Effect of *gyp7Δ* mutations on Vps10-mNG localisation. (A) Cells carrying the indicated combinations of gene deletions and genomic fluorescent tags were cultured, imaged and **(B)** quantified as in Figs. 2A and 2B.

Supplementary Figure 5. Ypt7 and Retromer are both predicted to bind Gyp6. (A) In silico screening of *S. cerevisiae* Retromer and Rab GAPs. The confidence score of potential interactors was assessed based on the sum of the iPTM score averaged from three AF2 and AF3 models. **(B)** Among the 9 yeast TBC domain containing GAPs, Gyp6 was confidently predicted to bind to Vps29 subunit of Retromer. **(C)** The PAE plots for the top ranked models of Ypt7 – Gyp6 and ctYpt7 – ctGyp6L complexes predicted by AlphaFold2. The iPTM score represents the averaged iPTM score from the three models. **(D)** Cartoon representation of the top ranked Ypt7 – Gyp6 and ctYpt7 – ctGyp6L complexes. GTP and Magnesium in the active site of Ypt7 were modelled based on the AF3 prediction. **(E)** Close view of Ypt7 – Gyp6 binding interface showing that Gyp6 recognize Ypt7 through canonical interaction.

Supplementary Figure 6. Gyp6 – Retromer colocalization. SEY6210 cells carrying genomically tagged Gyp6^{mNG} and Vps35^{yomCherry} were analysed by spinning disc fluorescence microscopy. Arrowheads indicate Gyp6^{mNG} and Vps35^{yomCherry} colocalising in the same structures. Scale bars: 5 μm.

Supplementary Figure 7. AlphaFold modelling of yeast Retromer and Gyp6 complex. (A) AF3- (left) and AF2- (right) predicted complex between Retromer and Gyp6, **(B)** ctRetromer and ctGyp6L, and **(C)** spRetromer – spGyp6. For AF3 prediction, the top three ranked models are aligned and shown in ribbon diagram. For AF2 prediction, only the top ranked model is shown. The models are coloured according the pLDDT confidence score. Panel on the left of the models shows the predicted alignment error (PAE) plots for the top-ranked prediction of the complex. The iPTM score represent the averaged iPTM score from the top three-ranked models.

Supplementary Figure 8. Comparison of the Vps29 - Gyp6^{TBC} models from three different yeast species. While all three Gyp6 models (left: Gyp6, middle: ctGyp6L, right: spGyp6) show a conserved TBC domain fold, they vary in the length of the loop containing the PL motif (highlighted in red).

Supplementary Figure 9. ITC measurement of Gyp6$^{105-122}$ and ctGyp6L$^{87-107}$ peptides binding to ctVps29. ITC graph shows the integrated and normalized data with a 1 to 1 ratio binding ratio.

Supplementary Figure 10. Crystal structure of ctGyp6L^{TBC} shows three distinct disordered loops. (A) Crystal structure of ctGyp6L^{TBC} solved at 2.1 Å resolution reveals two molecules in asymmetric unit. **(B)** Superimposition of the crystal structure and AF2 model highlighting the three distinct disordered loop observed in the structure.

Supplementary Figure 11. Sequence alignment of the Gyp6 C-terminal tail across the *Pezizomycotina* subdivision. *ct, Chaetomium thermophilum; vd, Verticillium dahlia; cm, Cordyceps militaris; nc, Neurospora crassa; mb, Metarhizium brunneum.* Blue arrow indicates the key residues involved in binding to Retromer.

Supplementary Figure 12. Design of LsmA-ctGyp6L$^{676-773}$ chimeric construct to enhance ctRetromer interaction. (A) Schematic diagram showing LsmA-ctGyp6L$^{676-773}$ chimera construct was designed by fusing ctGyp6L$^{676-773}$ to the C-terminus of full-length LsmA. **(B)** PAE plot showing the top-ranked AF2 models of LsmA-ctGyp6L$^{676-773}$ forming heptamer and **(C)** hexamer. **(D)** Cartoon representation of the top-ranked LsmA-ctGyp6L$^{676-773}$ heptamer (top) and hexamer (bottom). For clarity, the key LF motifs in ctGyp6L$_{676-77}$ are shown in sphere. **(E)** Superimposed view of LsmA-ctGyp6L$^{676-773}$ heptamer model with the previously determined crystal structure of LsmA (PDB ID: 1I81) showing that addition of ctGyp6L$^{676-773}$ does not affect LsmA oligomerization. **(F)** Mass photometry of LsmA-ctGyp6L$^{676-773}$ showing a size corresponds to the hexamer.

Table S1. Thermodynamic parameters for the binding of Retromer and Gyp6.

	K_d (μM)	ΔH (kcal/mol)	ΔG (kcal/mol)	$-T\Delta S$ (kcal/mol)
ctVps29				
Gyp6$^{105-122}$	1.42 ± 0.68	-7.40 ± 0.93	-8.15 ± 0.30	-0.87 ± 1.06
ctGyp6L^{TBC}	27.2 ± 5.52	-2.86 ± 0.28	-6.34 ±0.13	-3.46 ± 0.16
ctGyp6L$^{87-107}$		No binding detected		
ctVps29 + RT-D3				
Gyp6$^{105-122}$		No binding detected		
ctGyp6L^{TBC}		No binding detected		
ctRetromer				
ctGyp6L$^{680-698}$		No binding detected		
ctGyp6L$_{760-773}$		No binding detected		
LsmA-ctGYP6L$^{676-773}$ WT	5.8 ± 0.9	-11.7 ± 0.4	-7.3 ± 0.1	4.4 ± 0.5
LsmA-ctGYP6L$^{676-773}$ LF mutant		No binding detected		

Table S2. Summary of crystallographic structure determination statistics

Data collection statistics	ctGyp6L^{TBC}	mVPS29 – ctGyp6L$^{87-107}$	mVPS29 - Gyp6L$^{105-122}$
PDB ID	9Z83	9Z7E	9Z7D
Space group	P 1 21 1	C 2 2 21	P 1 21 1
Resolution (Å)	46.71 – 2.10	38.12 – 2.13	45.86 – 1.90
	(2.16 – 2.10)	(2.19 – 2.13)	(1.95 – 1.90)
a, b, c (Å)	47.93 128.42 64.50	44.40 72.12 114.36	56.86 43.35 77.31
α, β, γ (°)	90.00 102.92 90.00	90.00, 90.00, 90.00	90.00, 90.13 90.00
Total observations	301,587 (19,626)	94,146 (7,522)	96,263 (5,870)
Unique reflections	44,048 (3,139)	10,611 (7522)	29,385 (1,797)
Completeness (%)	98.8 (85.9)	99.8 (98.3)	98.3 (90.5)
R_{merge}^{+}	0.096 (1.619)	0.129 (1.403)	0.119 (1.486)
R_{pim*}	0.039 (0.685)	0.046 (0.484)	0.077 (0.950)
CC1/2	0.999 (0.562)	0.998 (0.627)	0.994 (0.278)
$\langle I/\sigma(I)\rangle$	10.0 (0.8)	9.9 (1.1)	6.6 (1.2)
Multiplicity	6.8 (6.3)	8.9 (9.1)	3.3 (3.3)
Molecule/asym	2	1	2
Refinement statistics			
R_{work}/R_{free} (%) ¶#	0.1888/0.2294	0.1899/0.2431	0.2636/0.2506
No. protein atoms	5,425	1,496	3,098
Waters	133	51	125
Average B (Å^2)^	51.13	48.37	33.25
Protein	51.04	48.29	33.35
Water	50.35	50.52	30.26
rmsd bonds (Å)	0.008	0.008	0.009
rmsd angles (°)	1.146	0.99	1.55
Ramachandran plot:			
Favored/outliers (%)	96.63/0.31	96.13/0.0	97.06/1.07

Values in parentheses refer to the highest resolution shell. $^{+}R_{merge} = \Sigma|I - \langle I\rangle| / \Sigma\langle I\rangle$, where I is the intensity of each individual reflection. $^{*}R_{pim}$ indicates all I^{+} & I^{-}. $^{¶}R_{work} = \Sigma h|F_o - F_c| / \Sigma_I|F_o|$, where F_o *and* F_c are the observed and calculated structure-factor amplitudes for each reflection *h*. $^{\#}R_{free}$ was calculated with 10% of the diffraction data selected randomly and excluded from refinement. ^Calculated using Baverage.

Table S3. Yeast strains used in the work.

Number	Strain	Genotype	Ref.
	BJ3505	MATα pep4::HIS3 prb1-Δ 1.6R lys2-208 trp1-Δ101 ura3-52 gal2 can	Lab
	SEY6210	MATα leu2-3,112 ura3-52 his3-Δ200 trp-Δ901 suc2-Δ9 lys2-801 GAL	Lab
CA239	BJ3505	ura3::pRS406 TetOffprom-TurboID-V5-Ypt7term	This study
CA240	BJ3505	ypt7Δ::KAN ura3::pRS406 TetOffprom-TurboID-V5-Ypt7-Ypt7term	This study
CA241	BJ3505	ypt7Δ::KAN ura3::pRS406 TetOffprom-TurboID-V5-ypt7^{Q68L}-Ypt7term	This study
CA242	BJ3505	ypt7Δ::KAN ura3::pRS406 TetOffprom-TurboID-V5-ypt7^{T22N}-Ypt7term	This study
CA260	SEY6210	Gyp6-mNeonGreen Vps35-yomCherry	This study
CA144	SEY6210	Vps10-mNeonGreen	This study
CA145	SEY6210	Vps10-mNeonGreen gyp3Δ	This study
CA220	SEY6210	Vps10-mNeonGreen gyp6Δ	This study
CA170	SEY6210	Vps10-mNeonGreen gyp7Δ	This study
CA221	SEY6210	Vps10-mNeonGreen gyp3Δ gyp6Δ	This study
CA223	SEY6210	Vps10-mNeonGreen gyp3Δ gyp6Δ gyp7Δ	This study
CA245	SEY6210	Vps10-mNeonGreen Vps35-yomCherry	This study
CA247	SEY6210	Vps10-mNeonGreen Vps35-yomCherry gyp3Δ gyp6Δ	This study
CA394	SEY6210	Vps35-mNeonGreen yomCherry-Ypt7	This study
CA395	SEY6210	Vps35-mNeonGreen yomCherry- ypt7^{Q68L}	This study
CA396	SEY6210	Vps35-mNeonGreen yomCherry-Ypt7 gyp3Δ gyp6Δ	This study
CA397	SEY6210	Vps35-mNeonGreen yomCherry- ypt7^{Q68L} gyp3Δ gyp6Δ	This study
CA263	SEY6210	Vps10-mNeonGreen ypt7Δ ura3::pRS406 Ypt7prom- ypt7^{Q68L}-Ypt7term gyp6Δ	This study
CA280	SEY6210	Vps10-mNeonGreen ypt7Δ ura3::pRS406 Ypt7prom- ypt7^{Q68L}-Ypt7term gyp3Δ	This study
CA282	SEY6210	Vps10-mNeonGreen ypt7Δ ura3::pRS406 Ypt7prom- ypt7^{Q68L}-Ypt7term gyp3Δ gyp6Δ	This study
CA288	SEY6210	Vps10-mNeonGreen ypt7Δ ura3::pRS406 Ypt7prom- ypt7^{Q68L}- Ypt7term gyp3Δ gyp6Δ leu2::pRS305-Gyp6prm-Gyp6-V5-CYC1term	This study
CA289	SEY6210	Vps10-mNeonGreen ypt7Δ ura3::pRS406 Ypt7prom- ypt7^{Q68L}-Ypt7term gyp3Δ gyp6Δ leu2::pRS305-Gyp6prm-Gyp6 R155A-V5-CYC1term	This study
CA314	SEY6210	Vps10-mNeonGreen ypt7Δ ura3::pRS406 Ypt7prom- ypt7^{Q68L}-Ypt7term gyp3Δ gyp6Δ leu2::pRS305-Gyp6prm-Gyp6 Δ415-458-V5-CYC1term	This study
CA323	SEY6210	Vps10-mNeonGreen ypt7Δ ura3::pRS406 Ypt7prom- ypt7^{Q68L}-Ypt7term gyp3Δ gyp6Δ leu2::pRS305-Gyp6prm-Gyp6 R108GL109GT110RV112GP119GL120A, Δ415-458-V5-CYC1term	This study
CA224	SEY6210	Vps10-mNeonGreen vps35Δ	This study
CA302	SEY6210	Vps10-mNeonGreen Vps35-yomCherry ypt7Δ ura3::pRS406 Ypt7prom- ypt7^{Q68L}-Ypt7term	This study
CA303	SEY6210	Vps10-mNeonGreen Vps35-yomCherry ypt7Δ ura3::pRS406 Ypt7prom- ypt7^{Q68L}-Ypt7term gyp3Δ gyp6Δ	This study
CA304	SEY6210	Vps10-mNeonGreen Vps35-yomCherry ypt7Δ ura3::pRS406 Ypt7prom- ypt7^{Q68L}-Ypt7term gyp3Δ gyp6Δ leu2::pRS305-Gyp6prm-Gyp6-V5-CYC1term	This study
CA305	SEY6210	Vps10-mNeonGreen Vps35-yomCherry ypt7Δ ura3::pRS406 Ypt7prom- ypt7^{Q68L}-Ypt7term gyp3Δ gyp6Δ leu2::pRS305-Gyp6prm-Gyp6 R155A-V5-CYC1term	This study
CA316	SEY6210	Vps10-mNeonGreen Vps35-yomCherry ypt7Δ ura3::pRS406 Ypt7prom- ypt7^{Q68L}-Ypt7term gyp3Δ gyp6Δ leu2::pRS305-Gyp6prm-Gyp6 Δ415-458-V5-CYC1term	This study
CA324	SEY6210	Vps10-mNeonGreen Vps35-yomCherry ypt7Δ ura3::pRS406 Ypt7prom- ypt7^{Q68L}-Ypt7term gyp3Δ gyp6Δ leu2::pRS305-Gyp6prm-Gyp6 R108GL109GT110RV112GP119GL120A, Δ415-458-V5-CYC1term	This study

Table S4: Plasmids used in the work.

Plasmids containing the sequence of the guide RNA for CrisperCas9 applications were produced with different auxotrophic markers, according to the strain.

Number	Plasmid Description	Reference
CA148	pRS406 Ypt7prom-Ypt7-Ypt7term	This study
CA149	pRS406 TetO-TurboID-Ypt7-Ypt7term	This study
CA150	pRS406 TetO-TurboID-Ypt7 Q68L-Ypt7term	This study
CA151	pRS406 TetO-TurboID-Ypt7 T22N-Ypt7term	This study
CA153	pRS406 TetO-TurboID-Ypt7term	This study
CA162	pRS305 Gyp6prom-Gyp6-V5-CYC1term	This study
CA163	pRS305 Gyp6prom-Gyp6 R155A-V5-CYC1term	This study
CA167	pRS406 Ypt7prom-Ypt7 Q68L-Ypt7term	This study
CA169	pRS305 Gyp6prom-Gyp6 R108GL109GT110RV112GP119GL120A-V5-CYC1term	This study
CA176	pRS305 Gyp6prom-Gyp6 Δ415-458-V5-CYC1term	This study
CA179	pRS305 Gyp6prom-Gyp6 R108GL109GT110RV112GP119GL120A, Δ415-458-V5-CYC1term	This study
pSP473	pRS423 *prGPD-cas9 his3*	Serge Pelet
pSP474	pRS423 *prGPD-cas9 trp1*	Serge Pelet
pSP475	pRS425 *prGPD-cas9 leu2*	Serge Pelet
pSP476	pRS426 *prGPD-cas9 ura3*	Serge Pelet

Table S5: Primers used in the work.

Number	Name	Sequence (5'-3')
CA081	Fw guide15 Ypt7	TCC CAA CAC CAG AGT CAC CTG TTT TAG AG
CA082	Rv guide15 Ypt7	CTA GCT CTA AAA CAG GTG ACT CTG GTG TTG GGA ACG T
CA237	Fw guide149 Gyp7	TAT CTC TAG CAT CGC TTG TTG TTT TAG AG
CA238	Rv guide149 Gyp7	CTA GCT CTA AAA CAA CAA GCG ATG CTA GAG ATA ACG T
CA299	Fw guide2 Gyp3	TTA CTT CAA GAT ACC TAC CGG TTT TAG AG
CA300	Rv guide2 Gyp3	CTA GCT CTA AAA CCG GTA GGT ATC TTG AAG TAA ACG T
	Fw guide2 Gyp6	TTTCGCTTATGCAACCATGAGTTTTAGAG
	Rv guide2 Gyp6	CTAGCTCTAAAACTCATGGTTGCATAAGCGAAAACGT
CA365	Fw guide173 Vps10	ATG TAA AGT AAT CTC TCT ACG TTT TAG AG
CA366	Rv guide173 Vps10	CTA GCT CTA AAA CGT AGA GAG ATT ACT TTA CAT ACG T
	Fw guide1 Vps35	GGGTGTTAGAATGTCTACAAGTTTTAGAG
	Rv guide1 Vps35	CTAGCTCTAAAAC TTGTAGACATTCTAACACCC ACGT
CA537	Fw guide34 vps35	CAC AAG TGC GTC GAA AAT GGG TTT TAG AG
CA538	Rv guide34 vps35	CTA GCT CTA AAA CCC ATT TTC GAC GCA CTT GTG ACG T
CA156	Fw Gyp7 del cassette	AAT TGG CAA AGT TCT ACA AGA GTC ATT CAT ACA TCC CCT GTG GTA AAT AGA AAC GGA ACT TTA CAT ATT GAA TAC CGG AG
CA157	Rv Gyp7 del cassette	CTC CGG TAT TCA ATA TGT AAA GTT CCG TTT CTA TTT ACC ACA GGG GAT GTA TGA ATG ACT CTTGTA GAA CTT TGC CAA TT
CA230	Fw Ypt7 del cassette	TCC ATA TAG AAA CCC CTT CTG TAT CAA TTC AAA TTA AGT GGC TGT ACT ACT TAA TTG TAT CTT CTA TTA TGT AAT CCT TT
CA231	Rv Ypt7 del cassette	AAA GGA TTA CAT AAT AGA AGA TAC AAT TAA GTA GTA CAG CCA CTT AAT TTG AAT TGA TAC AGA AGG GGT TTC TAT ATG GA
CA303	Fw Gyp3 del cassette	GGA GTC AAA GAG TTG CGC ACC CAG AAC CAT TGT AAT TAG CCT TTT GCT TCC TGT TTT TGT TTT TGC ATA AAC AAA TAT GT
CA304	Rv Gyp3 del cassette	ACA TAT TTG TTT ATG CAA AAA CAA AAA CAG GAA GCA AAA GGC TAA TTA CAA TGG TTC TGG GTG CGC AAC TCT TTG ACT CC
CA374	Fw Vps35 del cassette	TAA AAG GAG GAG GAC GAG AAA GAA GAA GCT GAA AAA CAC ATT AAA TAA CGT ACT TGC TCT TCG TAC ATG CCC AAG ATA AA
CA375	Rv Vps35 del cassette	TTT ATC TTG GGC ATG TAC GAA GAG CAA GTA CGT TAT TTA ATG TGT TTT TCA GCT TCT TCT TTC TCG TCC TCC TCC TTT TA
CA564	Fw Gyp6 del cassette	GTT AGC TGT CGT GCG TTT GTA TTT TTT CGC TTA TGC AAC AAG TTT TTC TTG TCA ATT ACT CGT TGT TAT TTG TTT GAA ATC
CA565	Rv Gyp6 del cassette	GAT TTC AAA CAA ATA ACA ACG AGT AAT TGA CAA GAA AAA CTT GTT GCA TAA GCG AAA AAA TAC AAA CGC ACG ACA GCT AAC
CA380	Fw mNG-Vps10 guide173	CTA CAG CGC CAT CTA ACG AAA AAC AGG GTG GTA GTG GTG GTG G
CA381	Rv Vps10 guide173	TTG TTT ATG AAA AGT ATA TGG AAT TAT CTA CTC TAT GTA AAG TAA TCT CTT TAC TTG TAC AAT TCG TCC ATA CC
CA395	Fw mNG-Gyp6 Guide 2	CAT AGA GAG GGT TAG CTG TCG TGC GTT TGT ATT TTT TCG CTT ATG CAA CAA TGG TCT CTA AGG GTG AAG AAG
CA396	Rv mNG-Gyp6 Guide 2	TTG GTC TCT TGT CTC GTA GTG GTC AAT CGC CCA TTG TAA GAC ATC CTT CAT GCC GCT ACC ACC AC
CA540	Fw Vps35-mNG guide34	GTA TAT CCC AAT ACA TCA TTT TCG ACG CAC TTG TGA GTA CAT TGA AAG TCA AAG AGA AGT TGA CGA TCG TTT CAA AGT CAT ATA TGT AGG TGG TAG TGG TGG TGG
CA541	Rv Vps35-mNG guide34	TTT ATC TTG GGC ATG TAC GAA GAG CAA GTA CGT TAT TTA ATT Act tgt aca att cgt cca tac cc
CA586	Rv yomCherry-Vps35 guide34	TTT ATC TTG GGC ATG TAC GAA GAG CAA GTA CGT TAT TTA ATT ACT TGT ACA GTT CAT CCA TAC CA

CA618	Fw -40bp yomCherry-Ypt7 guide15	TCC ATA TAG AAA CCC CTT CTG TAT CAA TTC AAA TTA AGT GAT GGT TAG CAA AGG CGA GG
CA619	Rv yomCherry-linker-Ypt7	CGA TGA ATT CTC TGT CGG ACC AGC ACC GGC ACC GGC ACC AGC ACC GGC ACC AGC ACC CTT GTA CAG TTC ATC CAT ACC ACC
CA163	Fw GFP ypt7 gen tag	CTT ATC CAT ATA GAA ACC CCT TCT GTA TCA ATT CAA ATT AAG TGA TGT CTA AAG GTG AAG AAT TAT TCA CTG G
CA294	Rv mNG-Ypt7 Guide15	AGA GTC ACC TAG TAT GAT TAC TTT CAA AAT ATT TTT TTT TCT AGA AGA CAT GCC GCT ACC ACC AC

REFERENCES

Adams PD, Afonine PV, Bunkoczi G, Chen VB, Davis IW, Echols N, Headd JJ, Hung LW, Kapral GJ, Grosse-Kunstleve RW, *et al* (2010) PHENIX: a comprehensive Python-based system for macromolecular structure solution. *Acta Crystallogr Sect D: Biol Crystallogr* 66: 213–21

Albert S & Gallwitz D (1999) Two new members of a family of Ypt/Rab GTPase activating proteins. Promiscuity of substrate recognition. *J Biol Chem* 274: 33186–9

Albert S, Will E & Gallwitz D (1999) Identification of the catalytic domains and their functionally critical arginine residues of two yeast GTPase-activating proteins specific for Ypt/Rab transport GTPases. *EMBO J* 18: 5216–5225

Ali R, Brett CL, Mukherjee S & Rao R (2004) Inhibition of sodium/proton exchange by a Rab-GTPase-activating protein regulates endosomal traffic in yeast. *J Biol Chem* 279: 4498–4506

Antón-Plágaro C, Chen K, Guo Q, Liu M, Evans AJ, Lewis PA, Heesom KJ, Wilkinson KA, Collins BM & Cullen PJ (2025) Mapping of endosomal proximity proteomes reveals Retromer as a hub for RAB GTPase regulation. *Nat Commun* 16: 6990

Arlt H, Reggiori F & Ungermann C (2015) Retromer and the dynamin Vps1 cooperate in the retrieval of transmembrane proteins from vacuoles. *J Cell Sci* 128: 645–655

Ashkenazy H, Abadi S, Martz E, Chay O, Mayrose I, Pupko T & Ben-Tal N (2016) ConSurf 2016: an improved methodology to estimate and visualize evolutionary conservation in macromolecules. *Nucleic Acids Res* 44: W344-50

Balderhaar HJ, Arlt H, Ostrowicz C, Brocker C, Sundermann F, Brandt R, Babst M & Ungermann C (2010) The Rab GTPase Ypt7 is linked to retromer-mediated receptor recycling and fusion at the yeast late endosome. *J Cell Sci* 123: 4085–94

Barlocher K, Hutter CAJ, Swart AL, Steiner B, Welin A, Hohl M, Letourneur F, Seeger MA & Hilbi H (2017) Structural insights into Legionella RidL-Vps29 retromer subunit interaction reveal displacement of the regulator TBC1D5. *Nat Commun* 8: 1543

Branon TC, Bosch JA, Sanchez AD, Udeshi ND, Svinkina T, Carr SA, Feldman JL, Perrimon N & Ting AY (2018) Efficient proximity labeling in living cells and organisms with TurboID. *Nat Biotechnol* 36: 880–887

Brett CL, Plemel RL, Lobinger BT, Vignali M, Fields S & Merz AJ (2008) Efficient termination of vacuolar Rab GTPase signaling requires coordinated action by a GAP and a protein kinase. *J Cell Biol* 182: 1141–1151

Brunet S, Saint-Dic D, Milev MP, Nilsson T & Sacher M (2016) The TRAPP Subunit Trs130p Interacts with the GAP Gyp6p to Mediate Ypt6p Dynamics at the Late Golgi. *Front Cell Dev Biol* 4: 48

Cabrera M, Ostrowicz CW, Mari M, LaGrassa TJ, Reggiori F & Ungermann C (2009) Vps41 phosphorylation and the Rab Ypt7 control the targeting of the HOPS complex to endosome-vacuole fusion sites. *Mol Biol Cell* 20: 1937–1948

Chen KE, Guo Q, Hill TA, Cui Y, Kendall AK, Yang Z, Hall RJ, Healy MD, Sacharz J, Norwood SJ, *et al* (2021) De novo macrocyclic peptides for inhibiting, stabilizing, and probing the function of the retromer endosomal trafficking complex. *Sci Adv* 7: eabg4007

Chen KE, Healy MD & Collins BM (2019) Towards a molecular understanding of endosomal trafficking by Retromer and Retriever. *Traffic* 20: 465–478

Chen K-E, Tillu VA, Gopaldass N, Chowdhury SR, Leneva N, Kovtun O, Ruan J, Guo Q, Ariotti N, Mayer A, *et al* (2025) Molecular basis for the assembly of the Vps5-Vps17 SNX-BAR proteins with Retromer. *Nat Commun* 16: 3568

Cho KF, Branon TC, Udeshi ND, Myers SA, Carr SA & Ting AY (2020) Proximity labeling in mammalian cells with TurboID and split-TurboID. *Nat Protoc* 15: 3971–3999

Collins BM, Harrop SJ, Kornfeld GD, Dawes IW, Curmi PM & Mabbutt BC (2001) Crystal structure of a heptameric Sm-like protein complex from archaea: implications for the structure and evolution of snRNPs. *J Mol Biol* 309: 915–23

Cooper AA & Stevens TH (1996) Vps10p cycles between the late-Golgi and prevacuolar compartments in its function as the sorting receptor for multiple yeast vacuolar hydrolases. *J cell Biol* 133: 529–541

Courtellemont T, Leo MGD, Gopaldass N & Mayer A (2022) CROP: a retromer-PROPPIN complex mediating membrane fission in the endo-lysosomal system. *EMBO J* 41: e109646

Cox J & Mann M (2008) MaxQuant enables high peptide identification rates, individualized p.p.b.-range mass accuracies and proteome-wide protein quantification. *Nat Biotechnol* 26: 1367–1372

Cox J & Mann M (2012) 1D and 2D annotation enrichment: a statistical method integrating quantitative proteomics with complementary high-throughput data. *BMC Bioinform* 13 Suppl 16: S12

Cox J, Neuhauser N, Michalski A, Scheltema RA, Olsen JV & Mann M (2011) Andromeda: a peptide search engine integrated into the MaxQuant environment. *J Proteome Res* 10: 1794–1805

Crawley-Snowdon H, Yang J-C, Zaccai NR, Davis LJ, Wartosch L, Herman EK, Bright NA, Swarbrick JS, Collins BM, Jackson LP, *et al* (2020) Mechanism and evolution of the Zn-

fingernail required for interaction of VARP with VPS29. *Nature communications* 11: 5031–15

Cui Y, Carosi JM, Yang Z, Ariotti N, Kerr MC, Parton RG, Sargeant TJ & Teasdale RD (2018) Retromer has a selective function in cargo sorting via endosome transport carriers. *J Cell Biol* 218: 615–631

Distefano MB, Haugen LH, Wang Y, Perdreau-Dahl H, Kjos I, Jia D, Morth JP, Neefjes J, Bakke O & Progida C (2018) TBC1D5 controls the GTPase cycle of Rab7b. *J Cell Sci* 131: jcs216630

Elbaz-Alon Y, Rosenfeld-Gur E, Shinder V, Futerman AH, Geiger T & Schuldiner M (2014) A dynamic interface between vacuoles and mitochondria in yeast. *Dev Cell* 30: 95–102

Evans PR & Murshudov GN (2013) How good are my data and what is the resolution? *Acta Crystallogr Sect D* 69: 1204–1214

Feng Y, Press B & Wandinger-Ness A (1995) Rab 7: an important regulator of late endocytic membrane traffic. *J cell Biol* 131: 1435–1452

Fukuda M (2011) TBC proteins: GAPs for mammalian small GTPase Rab? *Biosci Rep* 31: 159–68

Füllbrunn N, Nicastro R, Mari M, Griffith J, Herrmann E, Rasche R, Borchers A-C, Auffarth K, Kümmel D, Reggiori F, *et al* (2024) The GTPase activating protein Gyp7 regulates Rab7/Ypt7 activity on late endosomes. *J Cell Biol* 223: e202305038

Garrett MD, Zahner JE, Cheney CM & Novick PJ (1994) GDI1 encodes a GDP dissociation inhibitor that plays an essential role in the yeast secretory pathway. *EMBO J* 13: 1718–1728

Gonzalez-Lozano MA, Schmid EW, Whelan EM, Jiang Y, Paulo JA, Walter JC & Harper JW (2025) EndoMAP.v1 charts the structural landscape of human early endosome complexes. *Nature* 643: 1–10

Gopaldass N, Chen KE, Collins B & Mayer A (2024) Assembly and fission of tubular carriers mediating protein sorting in endosomes. *Nat Rev Mol Cell Biol* 25: 765–783

Gopaldass N, Leo MGD, Courtellemont T, Mercier V, Bissig C, Roux A & Mayer A (2023) Retromer oligomerization drives SNX-BAR coat assembly and membrane constriction. *EMBO J* 42: e112287

Guo Q, Chen K, Gimenez-Andres M, Jellett AP, Gao Y, Simonetti B, Liu M, Danson CM, Heesom KJ, Cullen PJ, *et al* (2024) Structural basis for coupling of the WASH subunit FAM21 with the endosomal SNX27–Retromer complex. *Proc Natl Acad Sci* 121: e2405041121

Haas AK, Fuchs E, Kopajtich R & Barr FA (2005) A GTPase-activating protein controls Rab5 function in endocytic trafficking. *Nat Cell Biol* 7: 887–93

Harrison MS, Hung CS, Liu TT, Christiano R, Walther TC & Burd CG (2014) A mechanism for retromer endosomal coat complex assembly with cargo. *Proc Natl Acad Sci* 111: 267–72

Healy MD, McNally KE, Butkovič R, Chilton M, Kato K, Sacharz J, McConville C, Moody ERR, Shaw S, Planelles-Herrero VJ, *et al* (2023) Structure of the endosomal Commander complex linked to Ritscher-Schinzel syndrome. *Cell* 186: 2219-2237.e29

Homma Y, Hiragi S & Fukuda M (2021) Rab family of small GTPases: an updated view on their regulation and functions. *FEBS J* 288: 36–55

Hönscher C, Mari M, Auffarth K, Bohnert M, Griffith J, Geerts W, Laan M van der, Cabrera M, Reggiori F & Ungermann C (2014) Cellular Metabolism Regulates Contact Sites between Vacuoles and Mitochondria. *Dev Cell* 30: 86–94

Jia D, Zhang J-S, Li F, Wang J, Deng Z, White MA, Osborne DG, Phillips-Krawczak C, Gomez TS, Li H, *et al* (2016) Structural and mechanistic insights into regulation of the retromer coat by TBC1d5. *Nat Commun* 7: 13305

Jimenez-Orgaz A, Kvainickas A, Nägele H, Denner J, Eimer S, Dengjel J & Steinberg F (2018) Control of RAB7 activity and localization through the retromer-TBC1D5 complex enables RAB7-dependent mitophagy. *EMBO J* 37: 235–254

Kabsch W (2010) Xds. *Acta Crystallogr Sect D: Biol Crystallogr* 66: 125–32

Kempen M van, Kim SS, Tumescheit C, Mirdita M, Lee J, Gilchrist CLM, Söding J & Steinegger M (2023) Fast and accurate protein structure search with Foldseek. *Nat Biotechnol* 42: 1–4

Kim DI, Birendra KC, Zhu W, Motamedchaboki K, Doye V & Roux KJ (2014) Probing nuclear pore complex architecture with proximity-dependent biotinylation. *Proc Natl Acad Sci* 111: E2453-61

Kovtun O, Leneva N, Bykov YS, Ariotti N, Teasdale RD, Schaffer M, Engel BD, Owen DJ, Briggs JAG & Collins BM (2018) Structure of the membrane-assembled retromer coat determined by cryo-electron tomography. *Nature* 561: 561–564

Kucharczyk R, Kierzek AM, Slonimski PP & Rytka J (2001) The Ccz1 protein interacts with Ypt7 GTPase during fusion of multiple transport intermediates with the vacuole in S. cerevisiae. *J Cell Sci* 114: 3137–45

Kulak NA, Pichler G, Paron I, Nagaraj N & Mann M (2014) Minimal, encapsulated proteomic-sample processing applied to copy-number estimation in eukaryotic cells. *Nat Methods* 11: 319–324

Kummel D, Herrmann E, Langemeyer L & Ungermann C (2023) Molecular insights into endolysosomal microcompartment formation and maintenance. *Biol Chem* 404: 441–454

Lachmann J, Barr FA & Ungermann C (2012) The Msb3/Gyp3 GAP controls the activity of the Rab GTPases Vps21 and Ypt7 at endosomes and vacuoles. *Mol Biol Cell* 23: 2516–2526

Lamber EP, Siedenburg A-C & Barr FA (2019) Rab regulation by GEFs and GAPs during membrane traffic. *Curr Opin Cell Biol* 59: 34–39

Lazar T, Scheglmann D & Gallwitz D (2002) A novel phospholipid-binding protein from the yeast Saccharomyces cerevisiae with dual binding specificities for the transport GTPase Ypt7p and the Sec1-related Vps33p. *Eur J Cell Biol* 81: 635–46

Leneva N, Kovtun O, Morado DR, Briggs JAG & Owen DJ (2021) Architecture and mechanism of metazoan retromer:SNX3 tubular coat assembly. *Sci Adv* 7: eabf8598

Liu T, Gomez TS, Sackey BK, Billadeau DD & Burd CG (2012) Rab GTPase regulation of retromer-mediated cargo export during endosome maturation. *Mol Biol Cell* 23: 2505–2515

Mccoy AJ, Grosse-Kunstleve RW, Adams PD, Winn MD, Storoni LC & Read RJ (2007) Phaser crystallographic software. *J Appl Crystallogr* 40: 658–674

Mirdita M, Schütze K, Moriwaki Y, Heo L, Ovchinnikov S & Steinegger M (2022) ColabFold: making protein folding accessible to all. *Nat Methods* 19: 679–682

Mirdita M, Steinegger M & Soding J (2019) MMseqs2 desktop and local web server app for fast, interactive sequence searches. *Bioinformatics* 35: 2856–2858

Modica G, Tejeda-Valencia L, Sauvageau E, Yasa S, Maes J, Skorobogata O & Lefrancois S (2025) Phosphorylation on serine 72 modulates Rab7A palmitoylation and retromer recruitment. *J Cell Sci* 138: jcs262177

Nickerson DP, Russell MRG, Lo SY, Chapin HC, Milnes J & Merz AJ (2012) Termination of isoform-selective Vps21/Rab5 signaling at endolysosomal organelles by Msb3/Gyp3. *Traffic* 13: 1411–1428

Nordmann M, Cabrera M, Perz A, Bröcker C, Ostrowicz C, Engelbrecht-Vandré S & Ungermann C (2010) The Mon1-Ccz1 complex is the GEF of the late endosomal Rab7 homolog Ypt7. *Curr Biol* 20: 1654–1659

Numrich J, Péli-Gulli M-P, Arlt H, Sardu A, Griffith J, Levine T, Engelbrecht-Vandré S, Reggiori F, Virgilio CD & Ungermann C (2015) The I-BAR protein Ivy1 is an effector of the Rab7 GTPase Ypt7 involved in vacuole membrane homeostasis. *J Cell Sci* 128: 2278–2292

Pan X, Eathiraj S, Munson M & Lambright DG (2006) TBC-domain GAPs for Rab GTPases accelerate GTP hydrolysis by a dual-finger mechanism. *Nature* 442: 303–306

Panicker N, Ge P, Dawson VL & Dawson TM (2021) The cell biology of Parkinson's disease. *J Cell Biol* 220: e202012095

Priya A, Kalaidzidis IV, Kalaidzidis Y, Lambright D & Datta S (2015) Molecular Insights into Rab7-Mediated Endosomal Recruitment of Core Retromer: Deciphering the Role of Vps26 and Vps35. *Traffic* 16: 68–84

Purushothaman LK, Arlt H, Kuhlee A, Raunser S & Ungermann C (2017) Retromer-driven membrane tubulation separates endosomal recycling from Rab7/Ypt7-dependent fusion. *Mol Biol Cell* 28: 783–791

Purushothaman LK & Ungermann C (2018) Cargo induces retromer-mediated membrane remodeling on membranes. *Mol Biol Cell* 29: 2709–2719

Pylypenko O, Hammich H, Yu IM & Houdusse A (2018) Rab GTPases and their interacting protein partners: Structural insights into Rab functional diversity. *Small GTPases* 9: 22–48

Qureshi YH, Baez P & Reitz C (2020) Endosomal Trafficking in Alzheimer's disease, Parkinson's Disease and Neuronal Ceroid Lipofuscinosis. *Mol Cell Biol* 40: e00262-20

Rojas R, Vlijmen T van, Mardones GA, Prabhu Y, Rojas AL, Mohammed S, Heck AJ, Raposo G, Sluijs P van der & Bonifacino JS (2008) Regulation of retromer recruitment to endosomes by sequential action of Rab5 and Rab7. *J Cell Biol* 183: 513–26

Romano-Moreno M, Rojas AL, Williamson CD, Gershlick DC, Lucas M, Isupov MN, Bonifacino JS, Machner MP & Hierro A (2017) Molecular mechanism for the subversion of the retromer coat by the Legionella effector RidL. *Proc Natl Acad Sci* 114: E11151–E11160

Schmid EW & Walter JC (2025) Predictomes, a classifier-curated database of AlphaFold-modeled protein-protein interactions. *Mol Cell* 85: 1216-1232.e5

Schwanhausser B, Busse D, Li N, Dittmar G, Schuchhardt J, Wolf J, Chen W & Selbach M (2011) Global quantification of mammalian gene expression control. *Nature* 473: 337–42

Seals DF, Eitzen G, Margolis N, Wickner WT & Price A (2000) A Ypt/Rab effector complex containing the Sec1 homolog Vps33p is required for homotypic vacuole fusion. *Proc Natl Acad Sci* 97: 9402–7

Seaman MN, Harbour ME, Tattersall D, Read E & Bright N (2009) Membrane recruitment of the cargo-selective retromer subcomplex is catalysed by the small GTPase Rab7 and inhibited by the Rab-GAP TBC1D5. *J Cell Sci* 122: 2371–82

Seaman MN, McCaffery JM & Emr SD (1998) A membrane coat complex essential for endosome-to-Golgi retrograde transport in yeast. *J Cell Biol* 142: 665–81

Seaman MNJ (2012) The retromer complex - endosomal protein recycling and beyond. *J Cell Sci* 125: 4693–4702

Stenmark H (2009) Rab GTPases as coordinators of vesicle traffic. *Nat Rev Mol Cell Biol* 10: 513–525

Strochlic TI, Setty TG, Sitaram A & Burd CG (2007) Grd19/Snx3p functions as a cargo-specific adapter for retromer-dependent endocytic recycling. *J Cell Biol* 177: 115–25

Stroupe C (2018) This Is the End: Regulation of Rab7 Nucleotide Binding in Endolysosomal Trafficking and Autophagy. *Front Cell Dev Biol* 6: 129

Suda Y, Kurokawa K, Hirata R & Nakano A (2013) Rab GAP cascade regulates dynamics of Ypt6 in the Golgi traffic. *Proc Natl Acad Sci* 110: 18976–81

Suzuki SW, Chuang YS, Li M, Seaman MNJ & Emr SD (2019) A bipartite sorting signal ensures specificity of retromer complex in membrane protein recycling. *J Cell Biol* 218: 2876–2886

Thomas LL, Highland CM & Fromme JC (2021) Arf1 orchestrates Rab GTPase conversion at the trans-Golgi network. *Mol Biol Cell* 32: 1104–1120

Vollmer P, Will E, Scheglmann D, Strom M & Gallwitz D (1999) Primary structure and biochemical characterization of yeast GTPase-activating proteins with substrate preference for the transport GTPase Ypt7p. *Eur J Biochem* 260: 284–90

Wichmann H, Hengst L & Gallwitz D (1992) Endocytosis in yeast: Evidence for the involvement of a small GTP-binding protein (Ypt7p). *Cell* 71: 1131–1142

Williams CJ, Headd JJ, Moriarty NW, Prisant MG, Videau LL, Deis LN, Verma V, Keedy DA, Hintze BJ, Chen VB, *et al* (2018) MolProbity: More and better reference data for improved all-atom structure validation. *Protein Sci* 27: 293–315

Wu C, Lin Y, Zheng H, Abubakar YS, Peng M, Li J, Yu Z, Wang Z, Naqvi NI, Li G, *et al* (2021) The retromer CSC subcomplex is recruited by MoYpt7 and sequentially sorted by MoVps17 for effective conidiation and pathogenicity of the rice blast fungus. *Mol Plant Pathol* 22: 284–298

Xie J, Heim EN, Crite M & DiMaio D (2020) TBC1D5-Catalyzed Cycling of Rab7 Is Required for Retromer-Mediated Human Papillomavirus Trafficking during Virus Entry. *Cell Rep* 31: 107750

Yao J, Yang F, Sun X, Wang S, Gan N, Liu Q, Liu D, Zhang X, Niu D, Wei Y, *et al* (2018) Mechanism of inhibition of retromer transport by the bacterial effector RidL. *Proc Natl Acad Sci* 115: E1446–E1454

Yong X, Mao L, Seaman MNJ & Jia D (2022) An evolving understanding of sorting signals for endosomal retrieval. *iScience* 25: 104254

Yong X, Mao L, Shen X, Zhang Z, Billadeau DD & Jia D (2021) Targeting Endosomal Recycling Pathways by Bacterial and Viral Pathogens. *Front Cell Dev Biol* 9: 648024

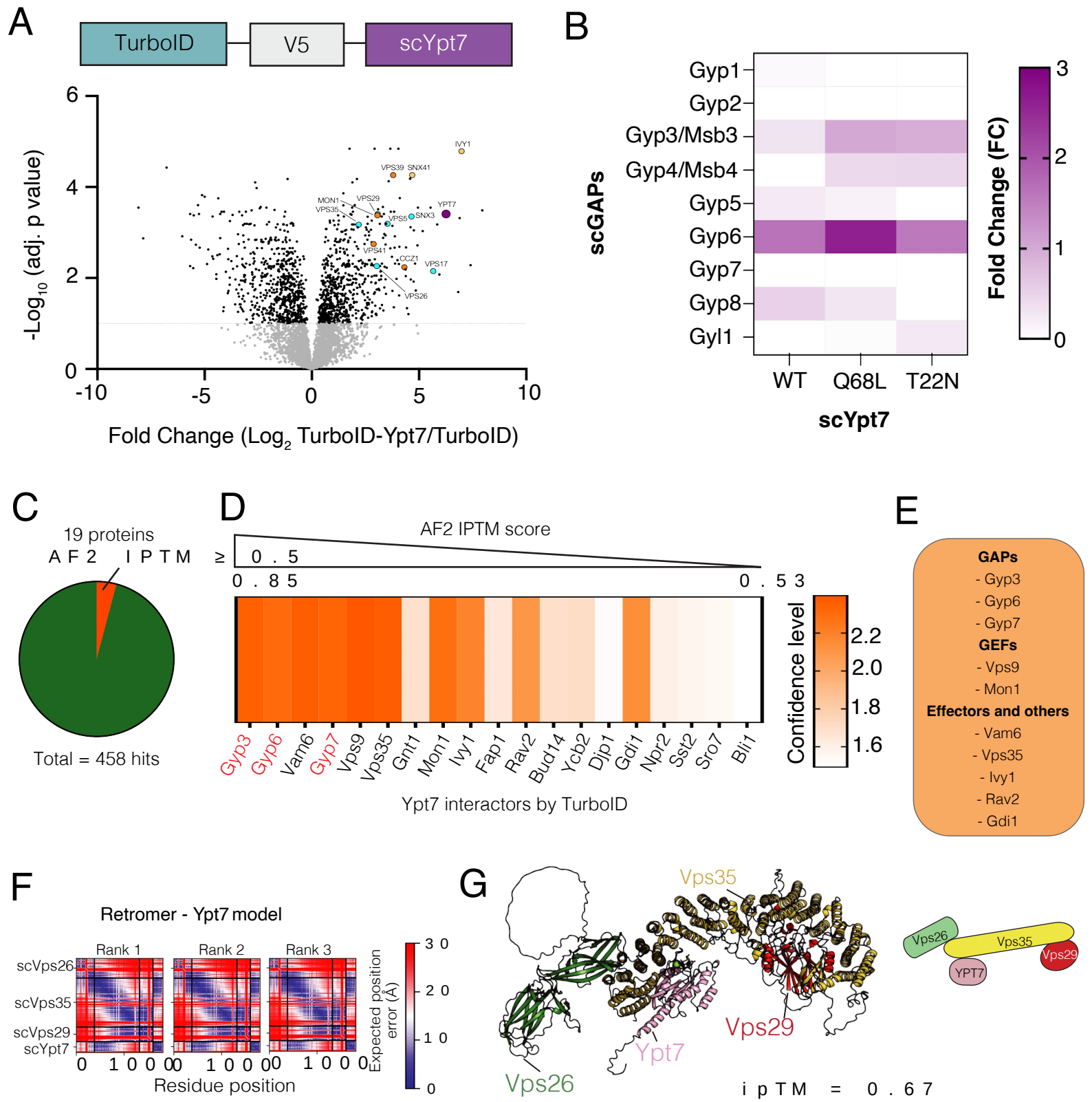
A
TurboID
V5
scYpt7
-Log10 (adj. p value)
Fold Change (Log2 TurboID-Ypt7/TurboID)
IVY1
VPS39
SNX41
MON1
VPS29
VPS35
YPT7
VPS5
SNX3
VPS41
CCZ1
VPS17
VPS26
B
scGAPs
Gyp1
Gyp2
Gyp3/Msb3
Gyp4/Msb4
Gyp5
Gyp6
Gyp7
Gyp8
Gyl1
WT
Q68L
T22N
scYpt7
Fold Change (FC)
C
19 proteins
AF2 IPTM ≥ 0.5
Total = 458 hits
D
AF2 IPTM score
0.85
0.53
Gyp3
Gyp6
Vam6
Gyp7
Vps9
Vps35
Gnt1
Mon1
Ivy1
Fap1
Rav2
Bud14
Ycb2
Djp1
Gdi1
Npr2
Sst2
Sro7
Bli1
Ypt7 interactors by TurboID
Confidence level
E
GAPs
- Gyp3
- Gyp6
- Gyp7
GEFs
- Vps9
- Mon1
Effectors and others
- Vam6
- Vps35
- Ivy1
- Rav2
- Gdi1
F
Retromer - Ypt7 model
Rank 1
Rank 2
Rank 3
scVps26
scVps35
scVps29
scYpt7
Residue position
Expected position error (Å)
G
Vps35
Vps29
Ypt7
Vps26
iptM = 0.67

Figure 1

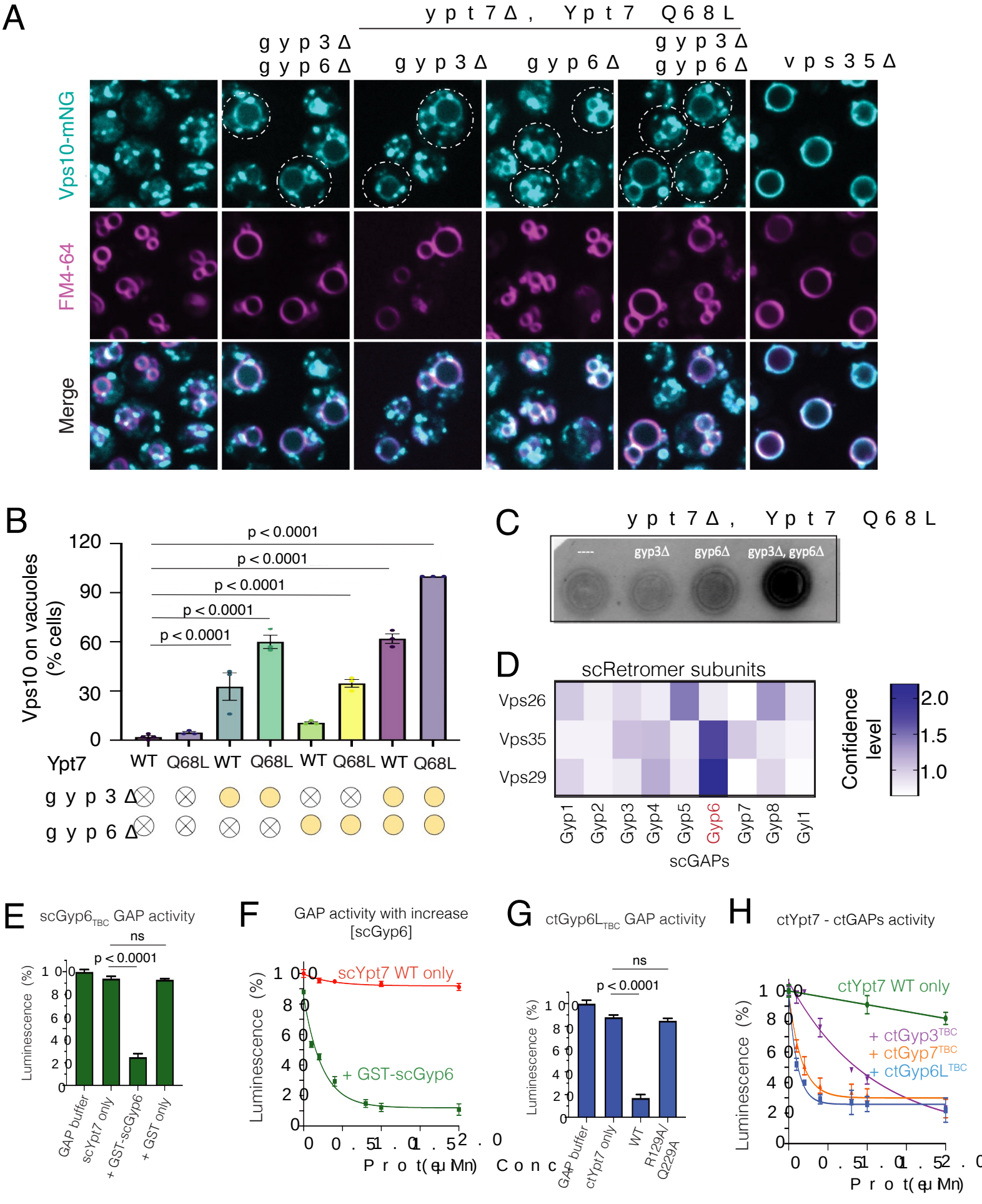
A
ypt7Δ, Ypt7 Q68L
gyp3Δ gyp6Δ
gyp3Δ
gyp6Δ
gyp3Δ gyp6Δ
vps35Δ
Vps10-mNG
FM4-64
Merge
B
Vps10 on vacuoles (% cells)
p < 0.0001
Ypt7
WT Q68L WT Q68L WT Q68L WT Q68L
gyp3Δ
gyp6Δ
C
ypt7Δ, Ypt7 Q68L
---
gyp3Δ
gyp6Δ
gyp3Δ, gyp6Δ
D
scRetromer subunits
Vps26
Vps35
Vps29
Gyp1 Gyp2 Gyp3 Gyp4 Gyp5 Gyp6 Gyp7 Gyp8 Gyl1
scGAPs
Confidence level
2.0
1.5
1.0
E
scGyp6TBC GAP activity
ns
p < 0.0001
Luminescence (%)
GAP buffer
scYpt7 only
+ GST-scGyp6
+ GST only
F
GAP activity with increase [scGyp6]
scYpt7 WT only
+ GST-scGyp6
Luminescence (%)
Prot Conc (μM)
G
ctGyp6LTBC GAP activity
ns
p < 0.0001
Luminescence (%)
GAP buffer
ctYpt7 only
WT
R129A/Q229A
H
ctYpt7 - ctGAPs activity
ctYpt7 WT only
+ ctGyp3TBC
+ ctGyp7TBC
+ ctGyp6LTBC
Luminescence (%)
Prot Conc (μM)

Figure 2

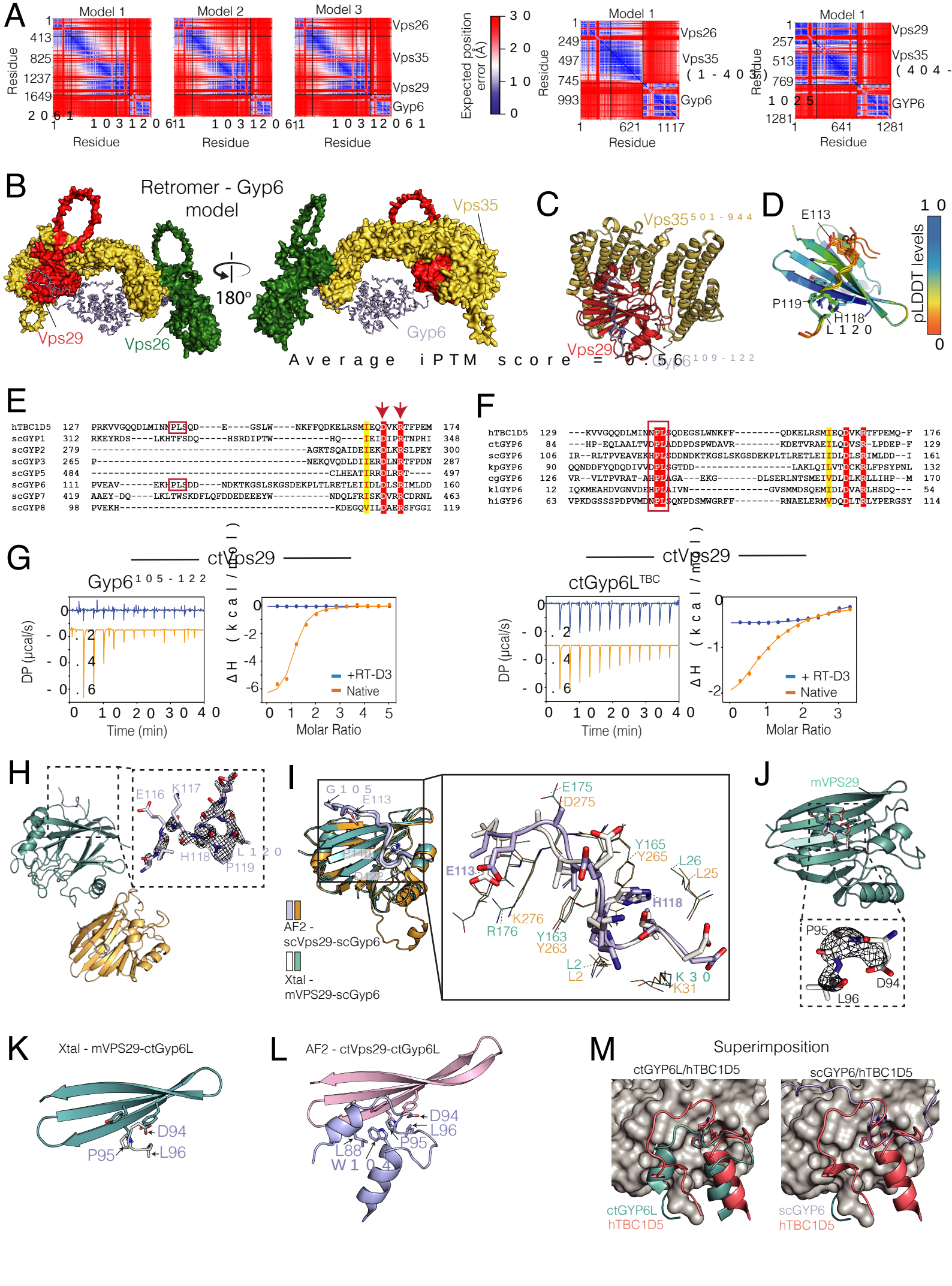
A
Model 1
Model 2
Model 3
Vps26
Vps35
Vps29
Gyp6
Residue
Expected position error (Å)
Model 1
Vps26
Vps35
(1-403)
Gyp6
Model 1
Vps29
Vps35
(404-1025)
GYP6
B
Retromer - Gyp6 model
Vps35
180°
Vps29
Vps26
Gyp6
Average iPTM score = 0.56
C
Vps35 501-944
Vps29
Gyp6 109-122
D
E113
P119
H118
L120
pLDDT levels
E
hTBC1D5 127 PRKVVGQQDLMINNPLSQD----E----GSLW----NKFFQDKELRSMIEQDVKRTFPEM 174
scGYP1 312 RKEYRDS----LKHTFSDQ-----HSRDIPTW----------HQ----IEIDIRTNPHI 348
scGYP2 279 ----------AGKTSQAIDEIEKDLKRSLPEY 300
scGYP3 265 P----------NEKQVQDLDIIERDLNRTFPDN 287
scGYP5 484 ----------CLHEATIRRDLRRT---- 497
scGYP6 111 PVEAV------EKHPLSDD----NDKTKGSLSKGSDEKPLTLRETLEIIDLDLSRIMLDD 160
scGYP7 419 AAEY-DQ----LKLTWSKDFLQFDDEDEEEYW----------NDQLFRISKDVRRCDRNL 463
scGYP8 98 PVEKH----------KDEGQVILDAERSFGGI 119
F
hTBC1D5 129 ---KVVGQQDLMINNPLSQDEGSLWNKFF--------QDKELRSMIEQDVKRTFPEMQ-F 176
ctGYP6 84 ---HP-EQLAALTVDPLADDPDSPWDAVR--------KDETVRAEILQDVSR-LPDEP-F 129
scGYP6 106 IR--RLTPVEAVEKHPLSDDNDKTKGSLSKGSDEKPLTLRETLEIIDLDLSRIMLDD--I 161
kpGYP6 90 QQNDDFYQDQDIVVDPLSGTDD----------LAKLQILVTDCKRLFPSYPNL 132
cgGYP6 126 VR--VLTPVRAT-AHPLAGA---EKG-------DLSERLNTSMEIVDLDLKRLLIHP--M 170
klGYP6 12 IQKMEAHDVGNVDEHPLAIVN----------GVSMMDSQEMIDLDVARLHSDQ--- 54
hiGYP6 63 VPKDGSSSPDPVMDNPLSQNPDSMWGRFF--------RNAELERMVDQDLTRLYPERGSY 114
G
ctVps29
Gyp6 105-122
DP (µcal/s)
Time (min)
ΔH (kcal/mol)
Molar Ratio
+RT-D3
Native
ctVps29
ctGyp6L TBC
DP (µcal/s)
Time (min)
ΔH (kcal/mol)
Molar Ratio
+ RT-D3
Native
H
E116
K117
H118
L120
P119
I
G105
E113
AF2 - scVps29-scGyp6
Xtal - mVPS29-scGyp6
E175
D275
Y165
Y265
L26
L25
E113
H118
K276
R176
Y163
Y263
L2
L2
K30
K31
J
mVPS29
P95
D94
L96
K
Xtal - mVPS29-ctGyp6L
D94
P95
L96
L
AF2 - ctVps29-ctGyp6L
D94
L96
P95
L88
W104
M
Superimposition
ctGYP6L/hTBC1D5
scGYP6/hTBC1D5
ctGYP6L
hTBC1D5
scGYP6
hTBC1D5

Figure 3

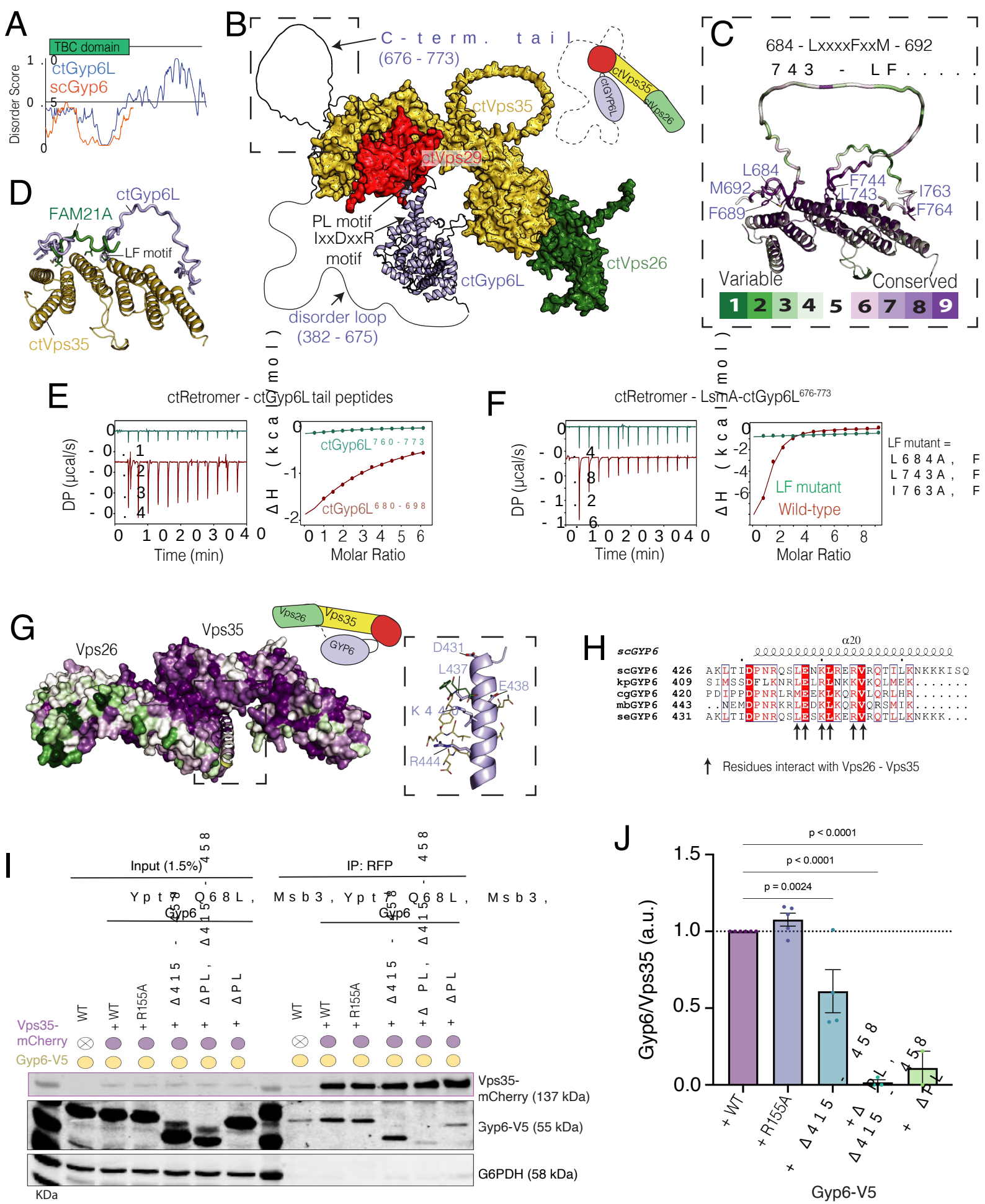
A
TBC domain
Disorder Score
ctGyp6L
scGyp6
B
C-term. tail
(676 - 773)
ctVps35
ctVps29
ctGYP6L
ctVps26
PL motif
IxxDxxR
motif
ctGyp6L
ctVps26
disorder loop
(382 - 675)
C
684 - LxxxxFxxM - 692
743 - LF.....
L684
M692
F689
F744
L743
I763
F764
Variable
Conserved
1 2 3 4 5 6 7 8 9
D
ctGyp6L
FAM21A
LF motif
ctVps35
E
ctRetromer - ctGyp6L tail peptides
DP (µcal/s)
Time (min)
ΔH (kcal/mol)
ctGyp6L 760-773
ctGyp6L 680-698
Molar Ratio
F
ctRetromer - LsmA-ctGyp6L 676-773
DP (µcal/s)
Time (min)
ΔH (kcal/mol)
LF mutant
Wild-type
Molar Ratio
LF mutant =
L684A, F
L743A, F
I763A, F
G
Vps26
Vps35
Vps26
Vps35
GYP6
D431
L437
E438
K440
R444
H
scGYP6
α20
scGYP6 426 AKLTIDPNRQSLENKLRERVRQTILKNKKKISQ
kpGYP6 409 SIMSSDFLKNRLELRLNKKVKQLMEK.....
cgGYP6 420 PDIPPDPNRLRMEEKLKQRVLQRLHR.....
mbGYP6 443 ..NEMDPNRKRLEDKLKQRVQRSMIK.....
seGYP6 431 AKLTIDPNRQSLESKLKERVRQTLLKNKKK...
Residues interact with Vps26 - Vps35
I
Input (1.5%)
IP: RFP
Ypt7 Q68L, Msb3, Ypt7 Q68L, Msb3,
Gyp6
Gyp6
WT
+ WT
+ R155A
+ Δ415 - 458
+ ΔPL, Δ415 - 458
+ ΔPL
Vps35-mCherry
Gyp6-V5
Vps35-mCherry (137 kDa)
Gyp6-V5 (55 kDa)
G6PDH (58 kDa)
KDa
J
p < 0.0001
p < 0.0001
p = 0.0024
Gyp6/Vps35 (a.u.)
+ WT
+ R155A
+ Δ415 - 458
+ ΔPL, Δ415 - 458
+ ΔPL
Gyp6-V5

Figure 4

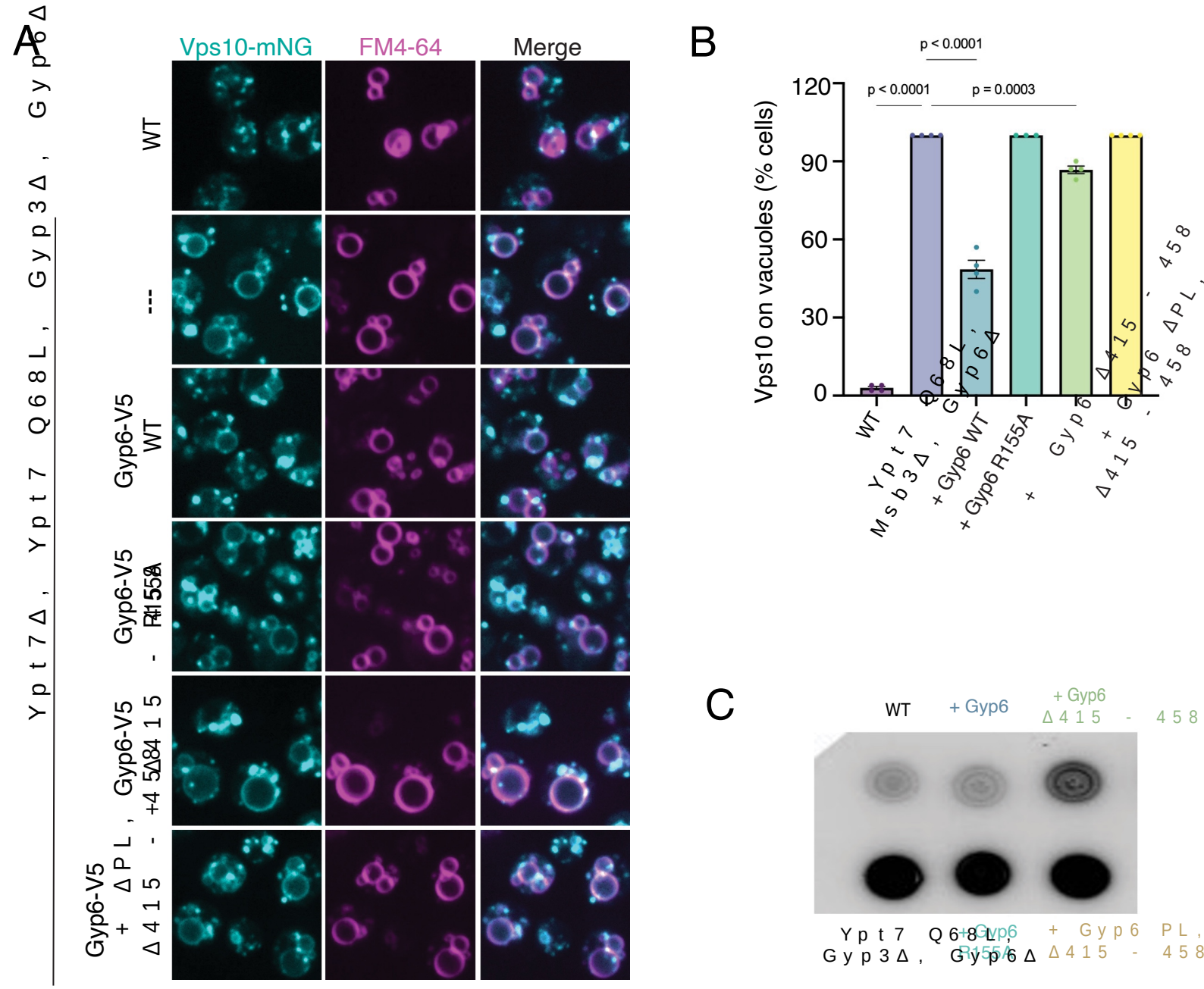
A
Vps10-mNG
FM4-64
Merge
WT

Gyp6-V5 WT
Gyp6-V5 R155A
Gyp6-V5 Δ415-458
Gyp6-V5 +ΔPL, Δ415-458
Ypt7Δ, Ypt7 Q68L, Gyp3Δ, Gyp6Δ
B
p < 0.0001
p < 0.0001
p = 0.0003
Vps10 on vacuoles (% cells)
120
90
60
30
0
WT
Ypt7 Msb3Δ, Gyp6Δ
Ypt7 Msb3Δ, Q68L, Gyp6Δ
+ Gyp6 WT
+ Gyp6 R155A
+ Gyp6 Δ415-458
+ Gyp6 Δ415-458 ΔPL
C
WT
+ Gyp6
+ Gyp6 Δ415-458
Ypt7 Gyp3Δ, Gyp6Δ
Ypt7 Q68L, Gyp3Δ, Gyp6Δ
+ Gyp6 R155A
+ Gyp6 Δ415-458
+ Gyp6 ΔPL, Δ415-458

Figure 5

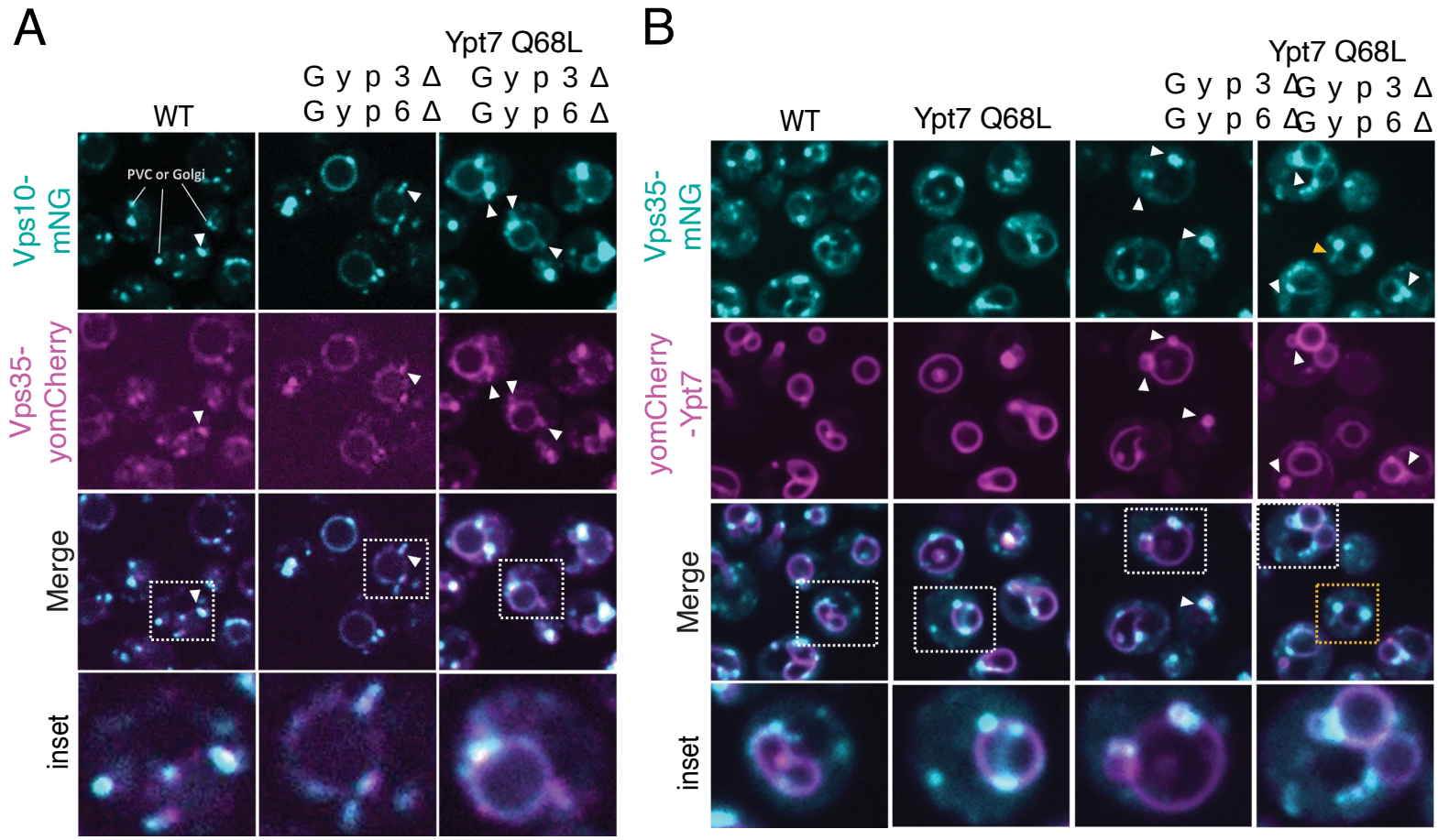
A
Ypt7 Q68L
WT
Gyp3Δ Gyp3Δ
Gyp6Δ Gyp6Δ
Vps10-mNG
PVC or Golgi
Vps35-yomCherry
Merge
inset
B
Ypt7 Q68L
WT
Ypt7 Q68L
Gyp3Δ Gyp3Δ
Gyp6Δ Gyp6Δ
Vps35-mNG
yomCherry-Ypt7
Merge
inset

Figure 6

A

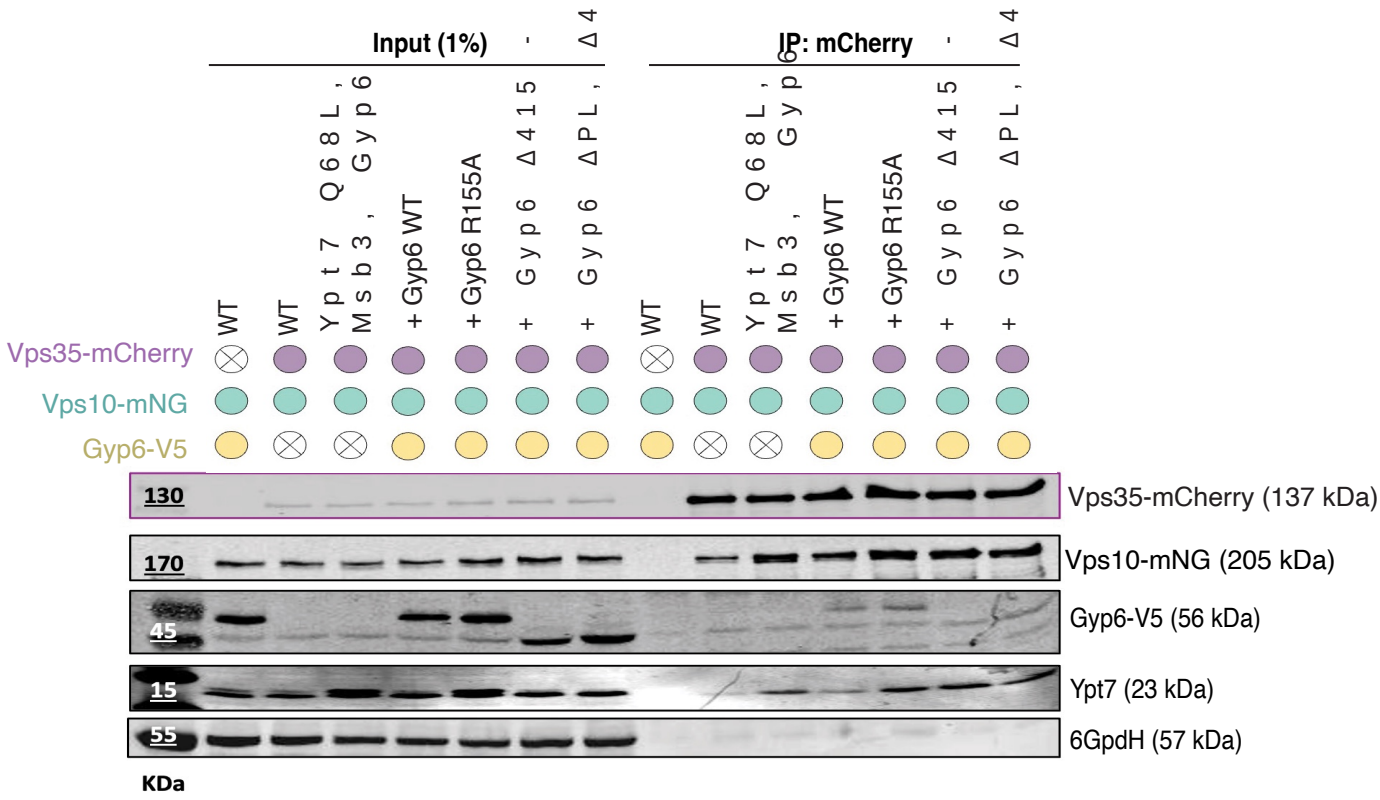
Input (1%)
IP: mCherry
WT
Ypt7 Q68L, Msb3Δ, Gyp6Δ
+ Gyp6 WT
+ Gyp6 R155A
+ Gyp6 Δ415
+ Gyp6 ΔPL, Δ458
Vps35-mCherry
Vps10-mNG
Gyp6-V5
130
170
45
15
55
KDa
Vps35-mCherry (137 kDa)
Vps10-mNG (205 kDa)
Gyp6-V5 (56 kDa)
Ypt7 (23 kDa)
6GpdH (57 kDa)

B

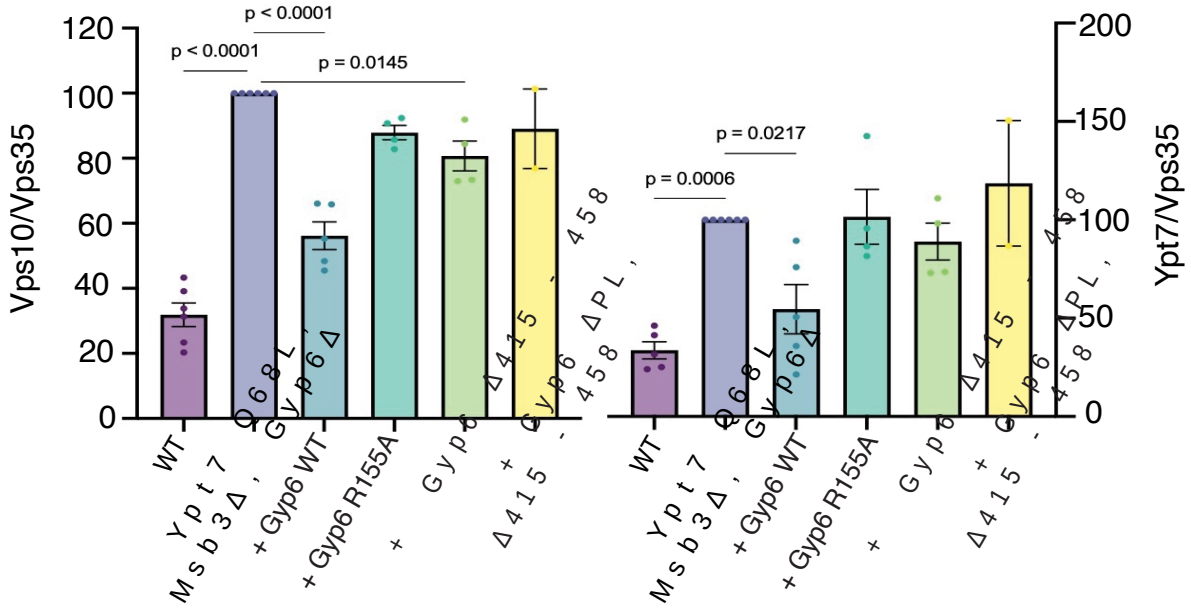
Vps10/Vps35
Ypt7/Vps35
p < 0.0001
p < 0.0001
p = 0.0145
p = 0.0006
p = 0.0217
WT
Ypt7 Msb3Δ, Q68L, Gyp6Δ
+ Gyp6 WT
+ Gyp6 R155A
+ Gyp6 Δ415
+ Gyp6 ΔPL, Δ458

Figure 7

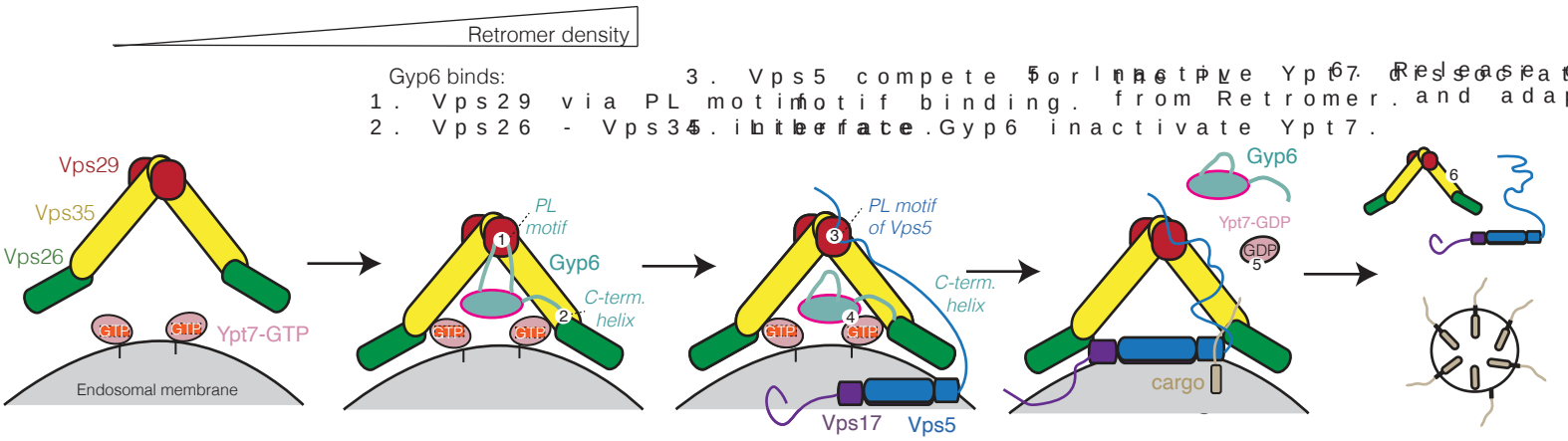

Recruitment of Retromer by active Ypt7

Recruitment of Gyp6 by Retromer via the PL motif and C-terminal tail helix interaction

Adaptor Vps5 - Vps17 competes for binding via the PL motif (with stronger affinity) and liberate Gyp6 to inactive Ypt7

GTP hydrolysis facilitates membrane fission and carrier release

Figure 8

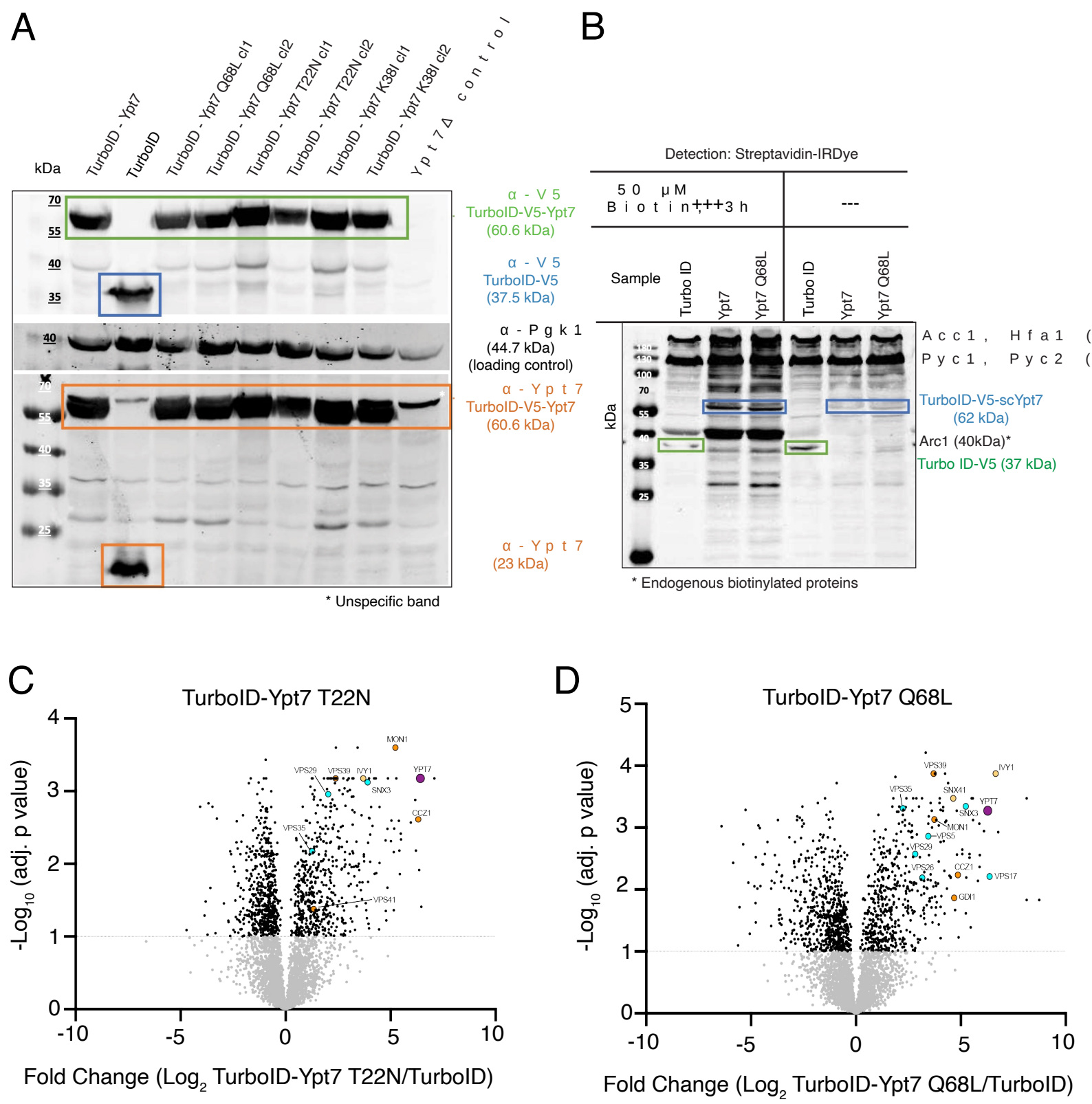

Supplementary Figure 1

S. cerevisiae Retromer - Ypt7^{GTP} model

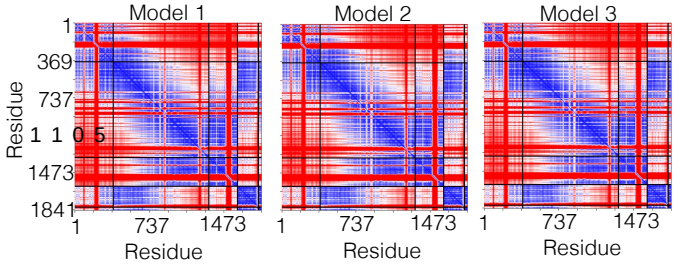

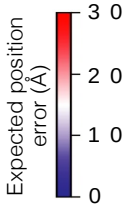

S. cerevisiae Ivy1 - Ypt7^{GTP} model

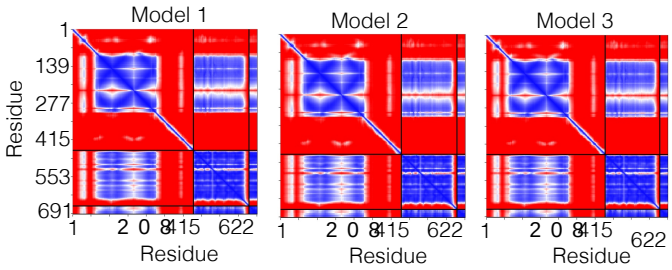

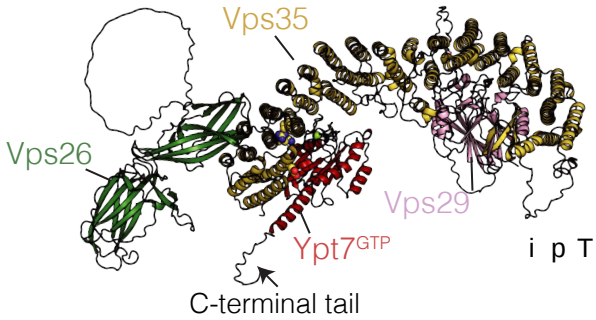

ipTM = 0.71

ipTM =

S. cerevisiae Gdi - Ypt7^{GDP} model

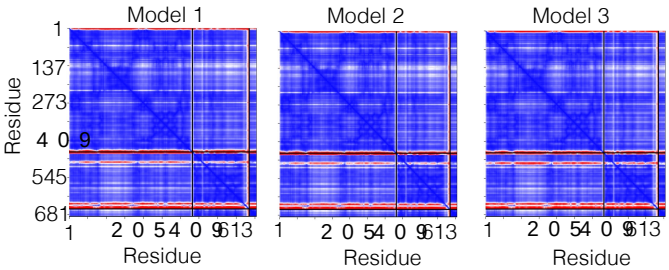

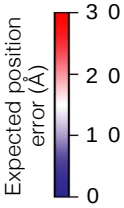

S. cerevisiae Mon1 - Ccz1 - Ypt7^{GDP} model

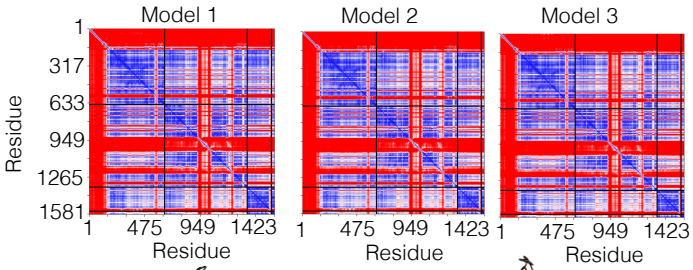

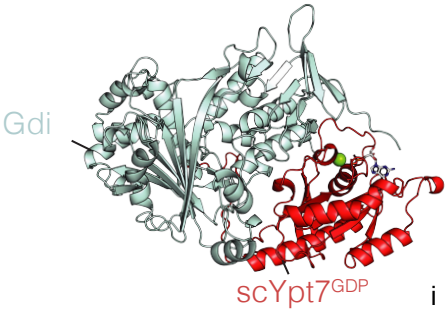

ipTM = 0.88

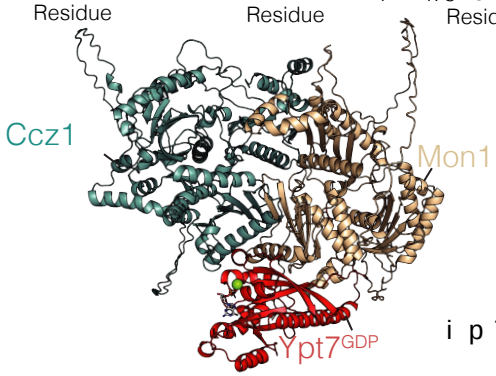

ipTM =

S. cerevisiae HOPS complex - Ypt7^{GTP} model

S. cerevisiae Vps39 - Ypt7^{GTP}

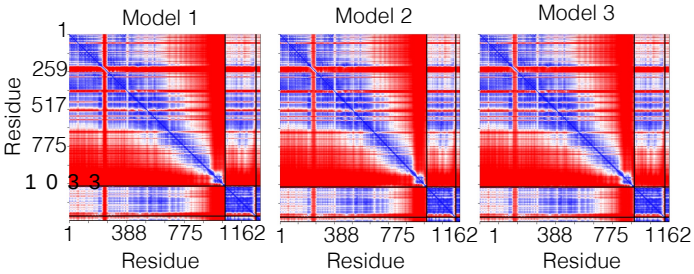

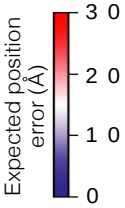

S. cerevisiae Vps41 - Ypt7^{GTP}

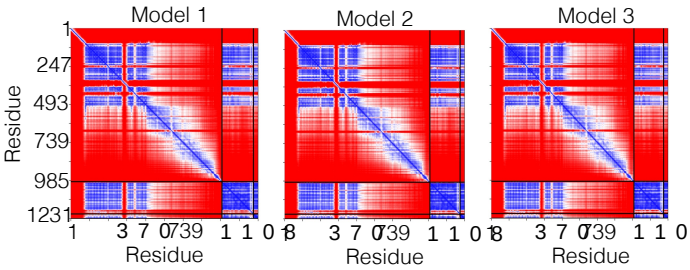

ipTM = 0.83

ipTM = 0.87

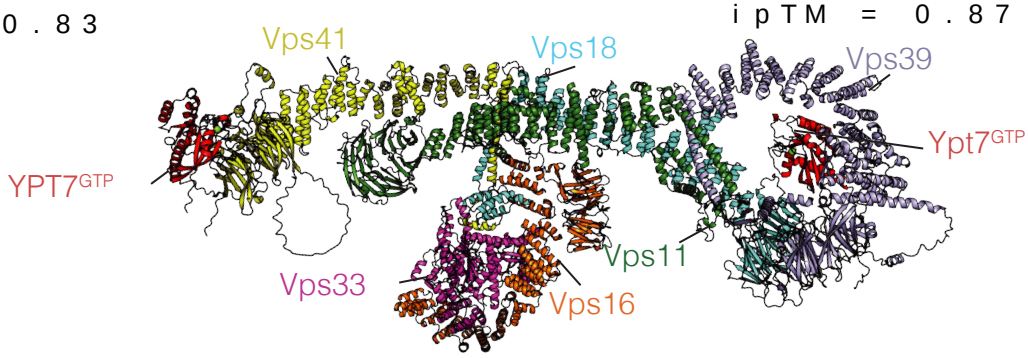

Supplementary Figure 2

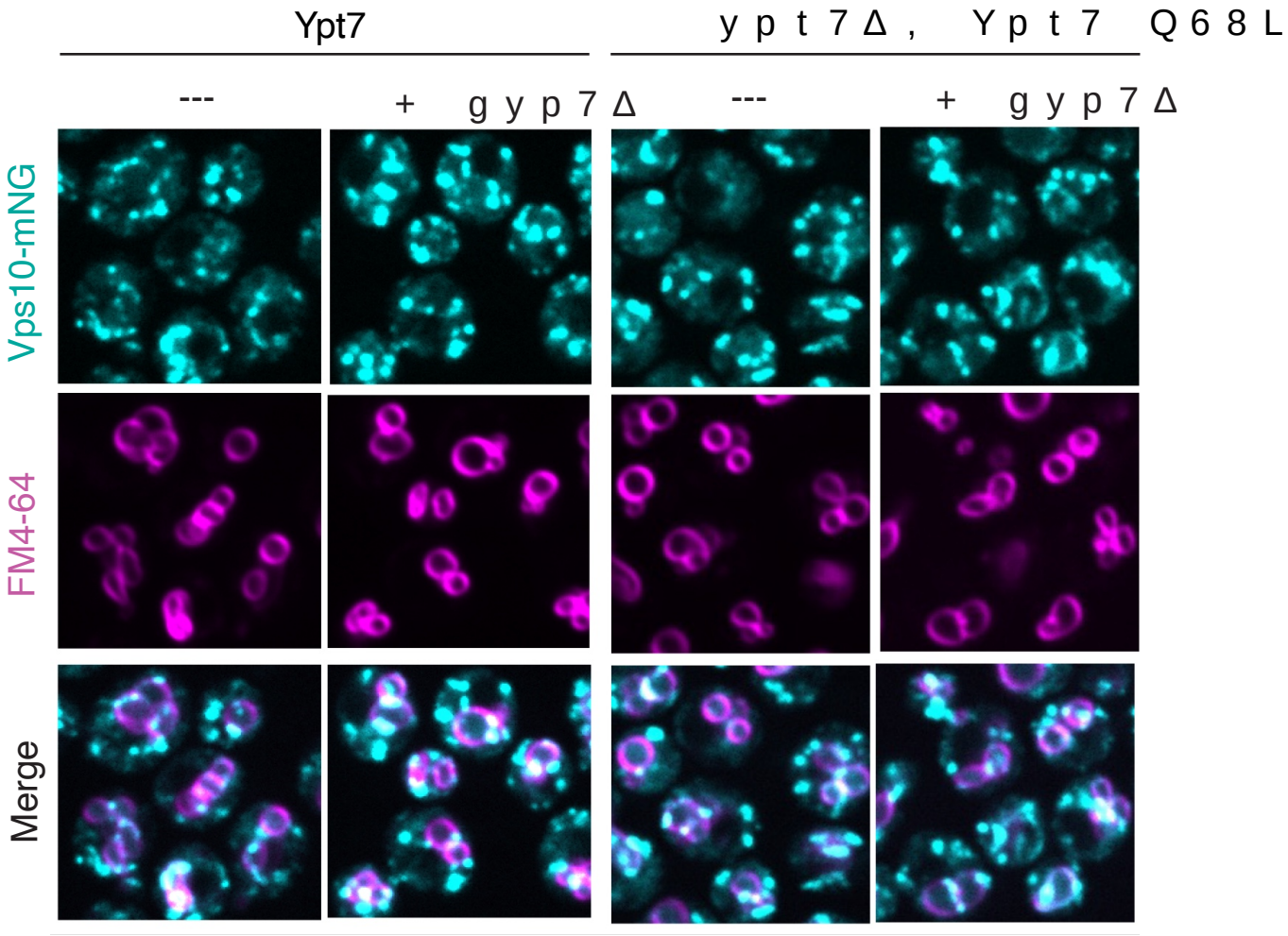

Supplementary Figure 3

A

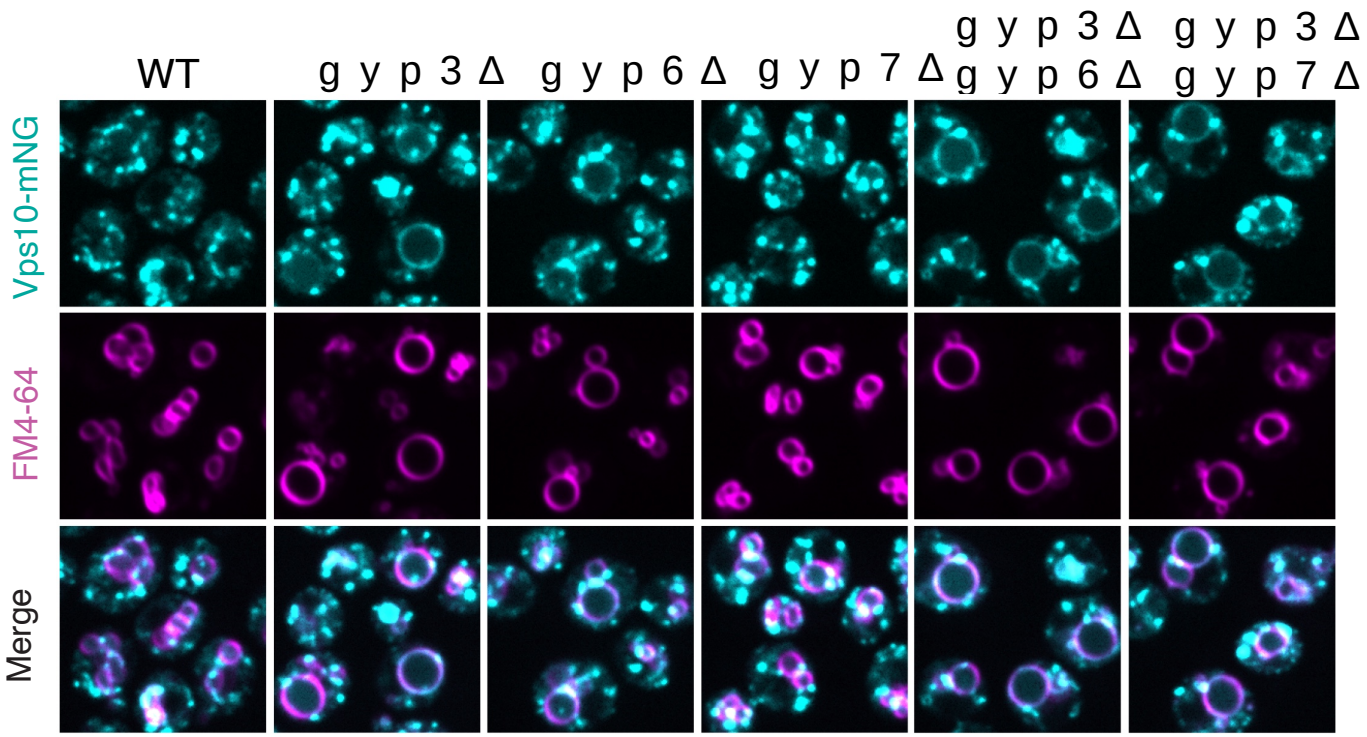

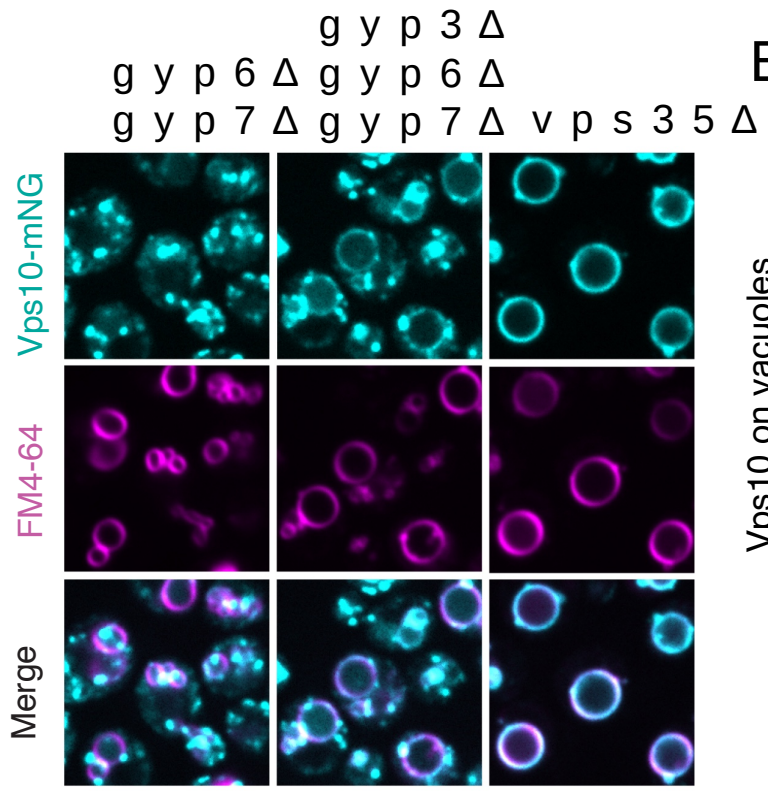

B

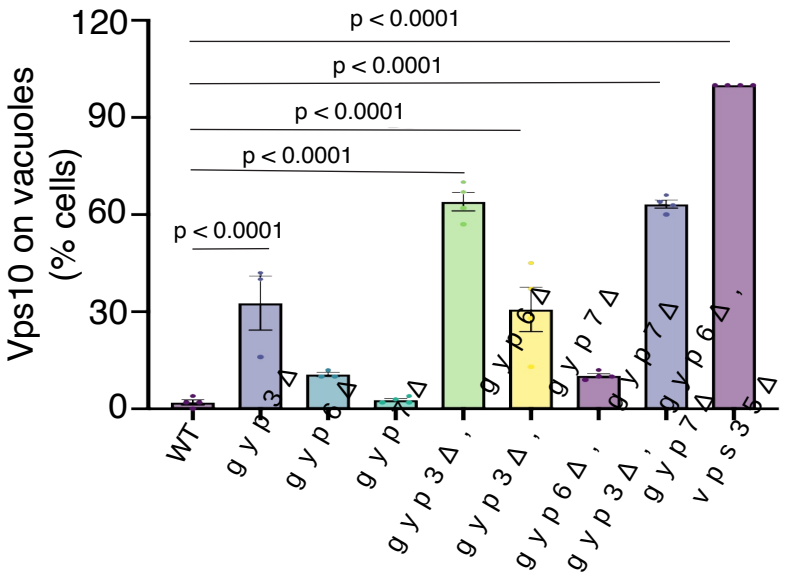

Supplementary Figure 4

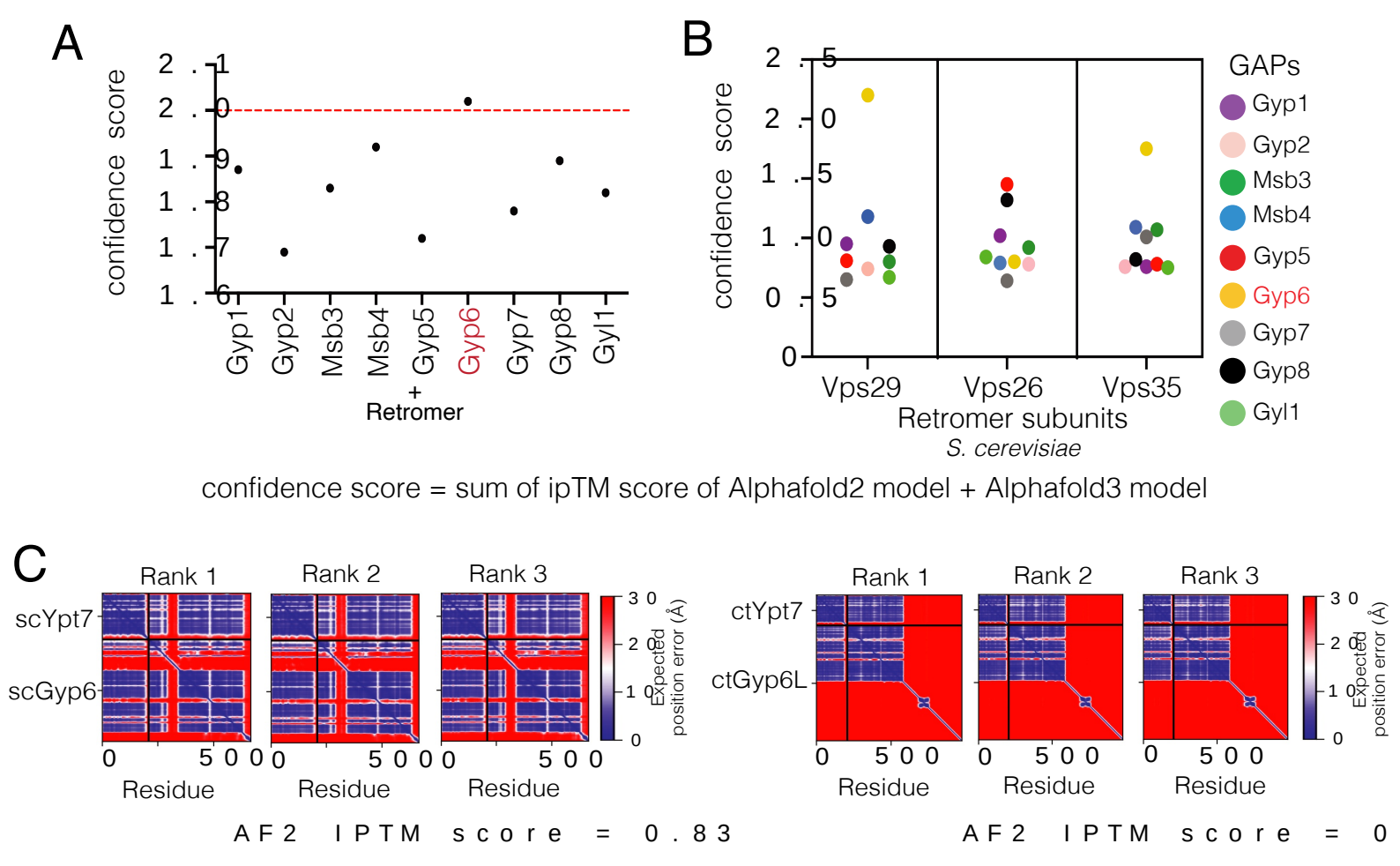

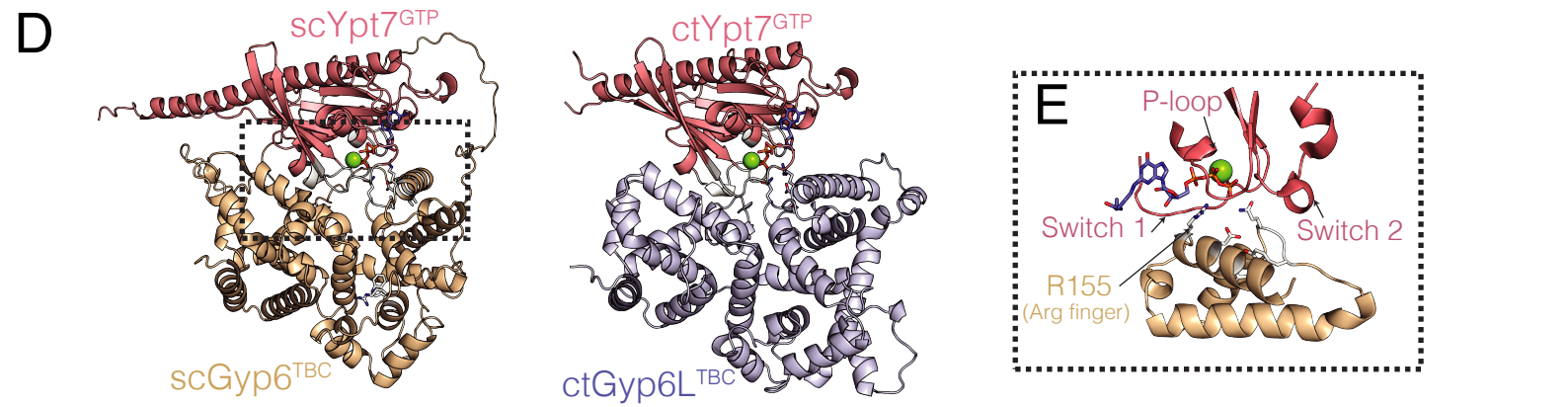

Supplementary Figure 5

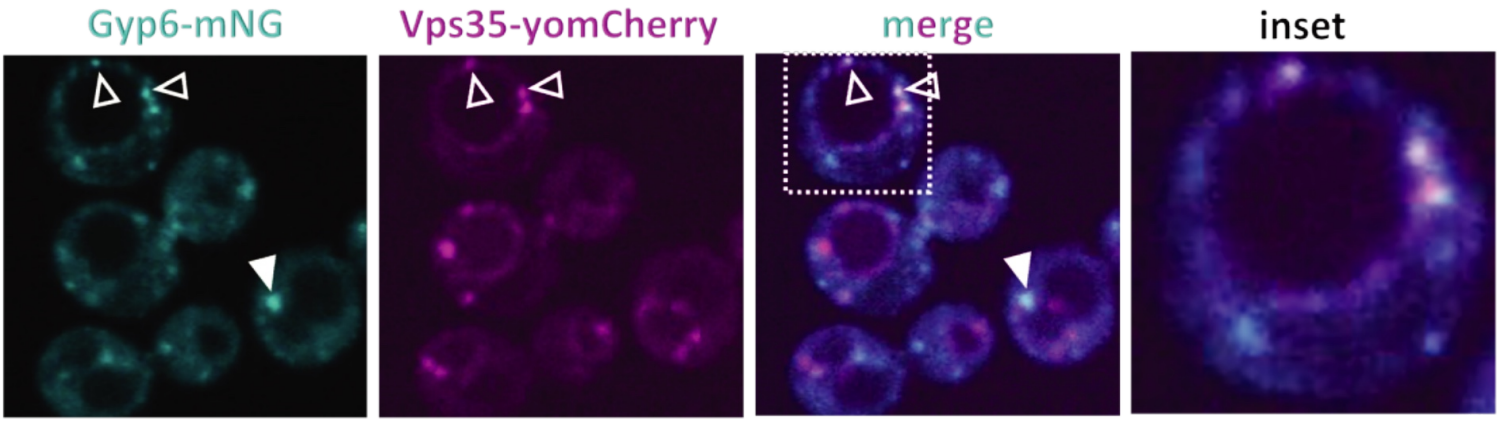

Supplementary Figure 6

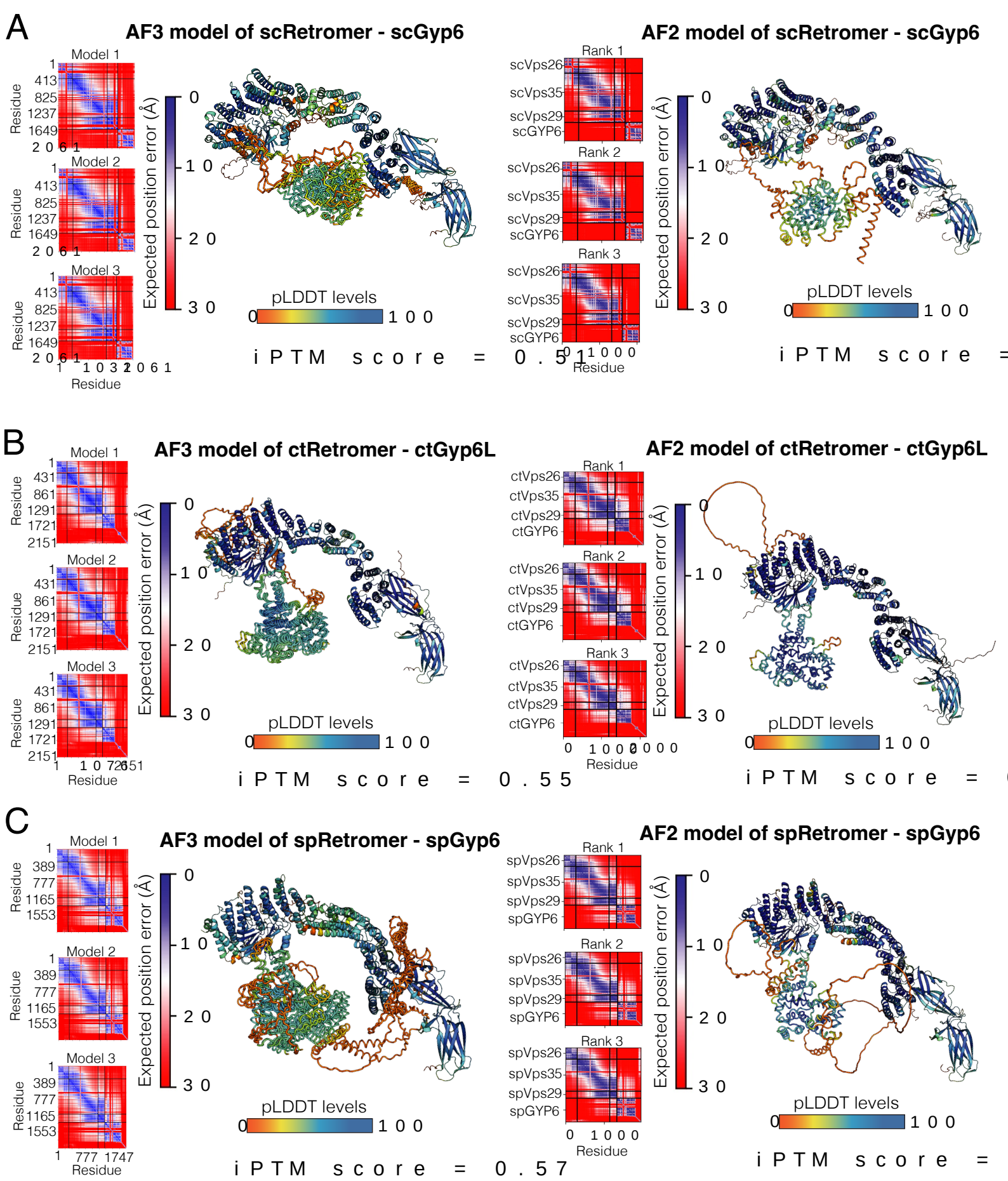

Supplementary Figure 7

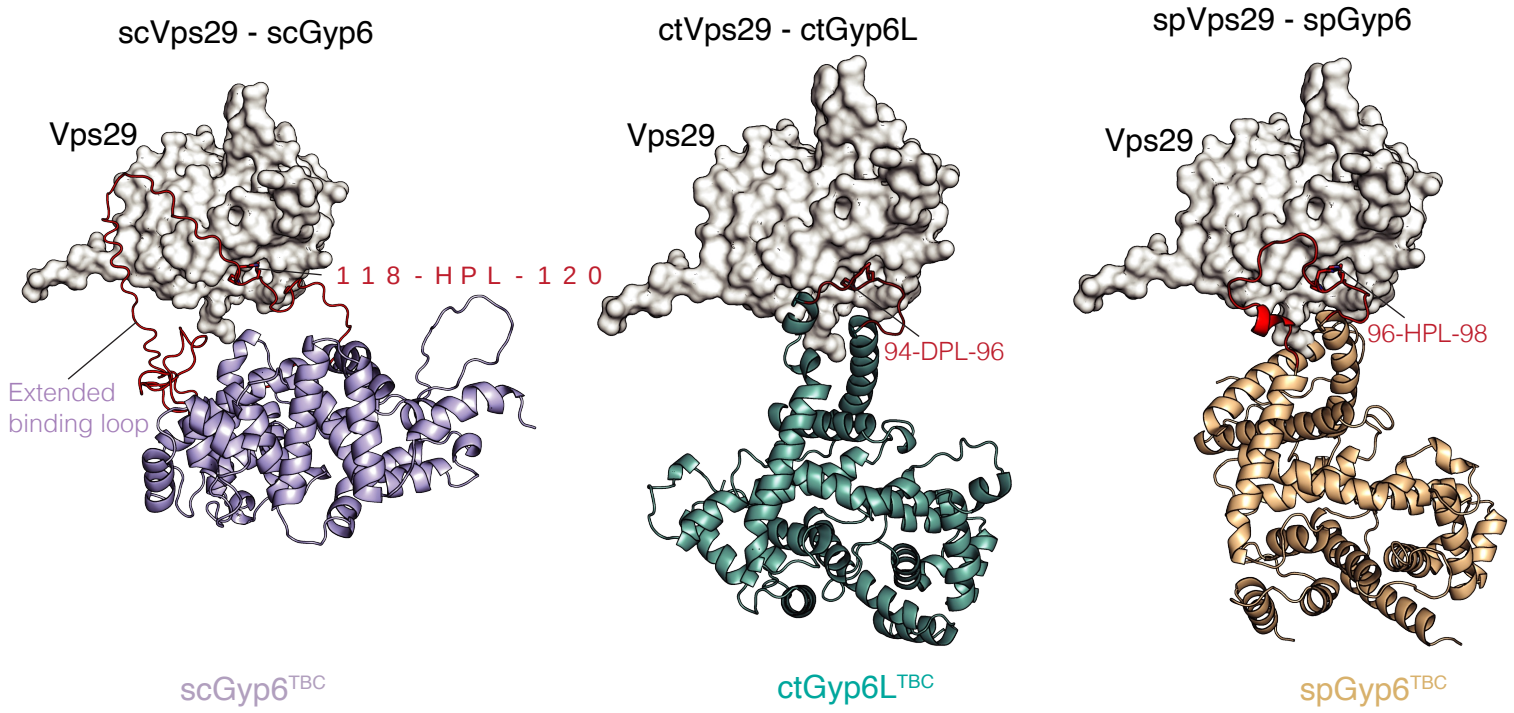

Supplementary Figure 8

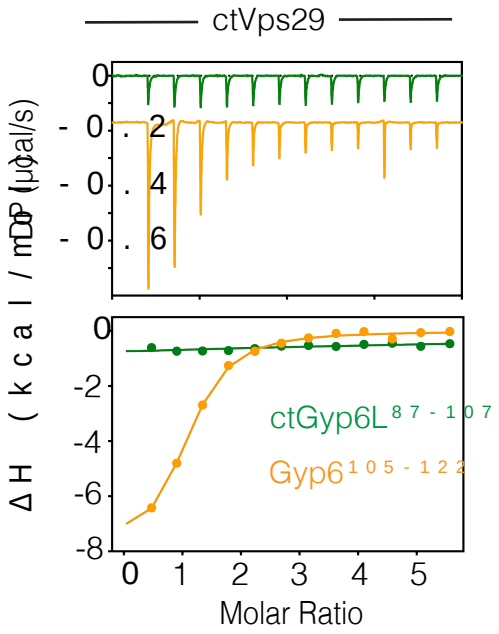

Supplementary Figure 9

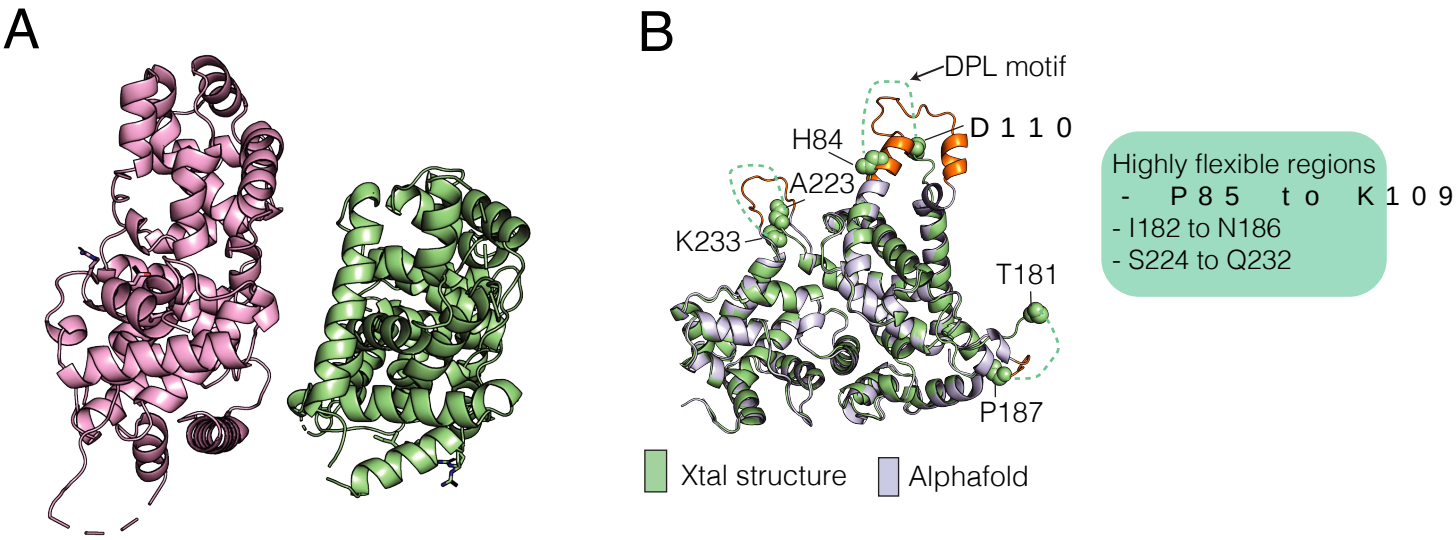

Supplementary Figure 10

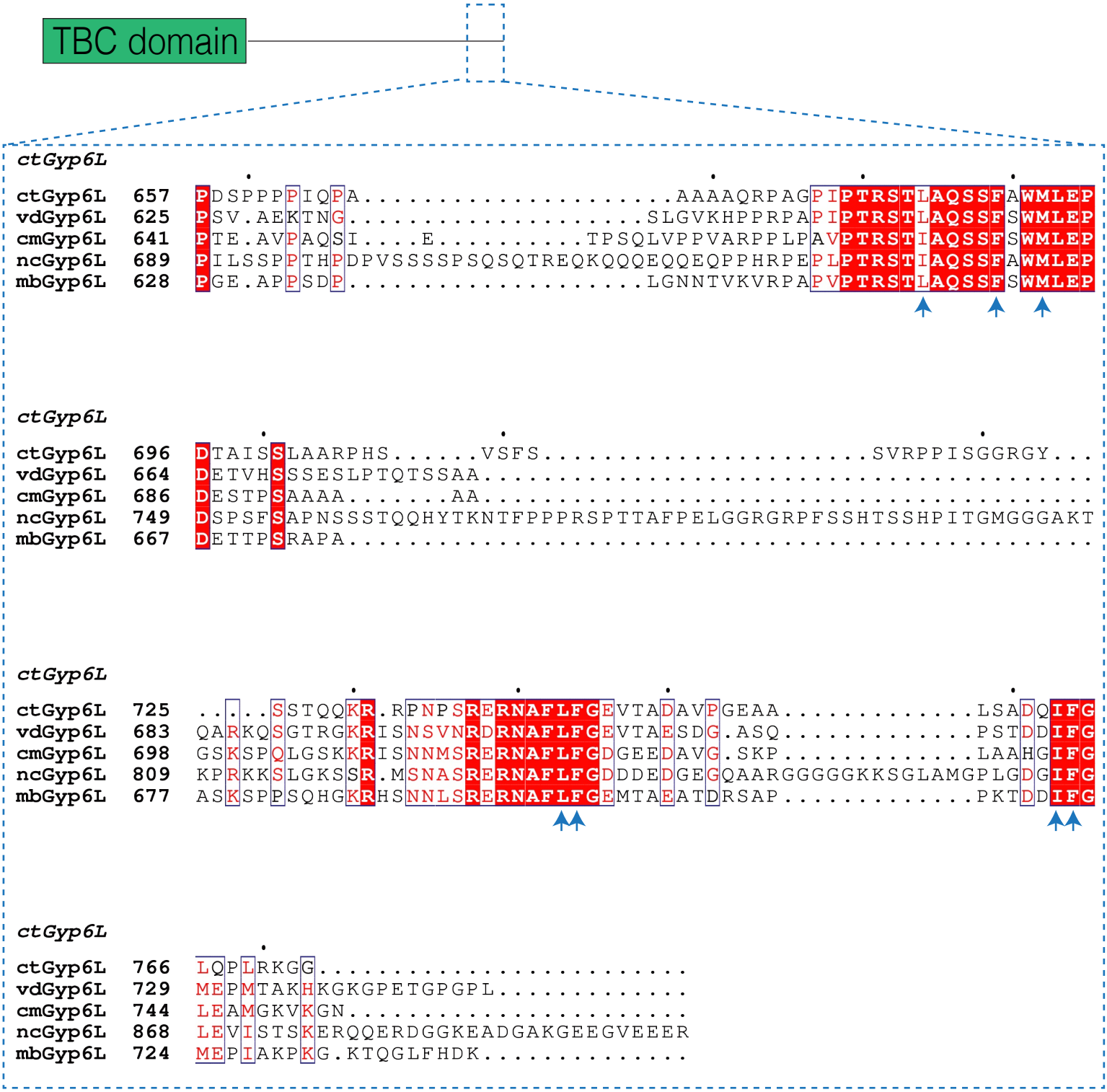

Supplementary Figure 11

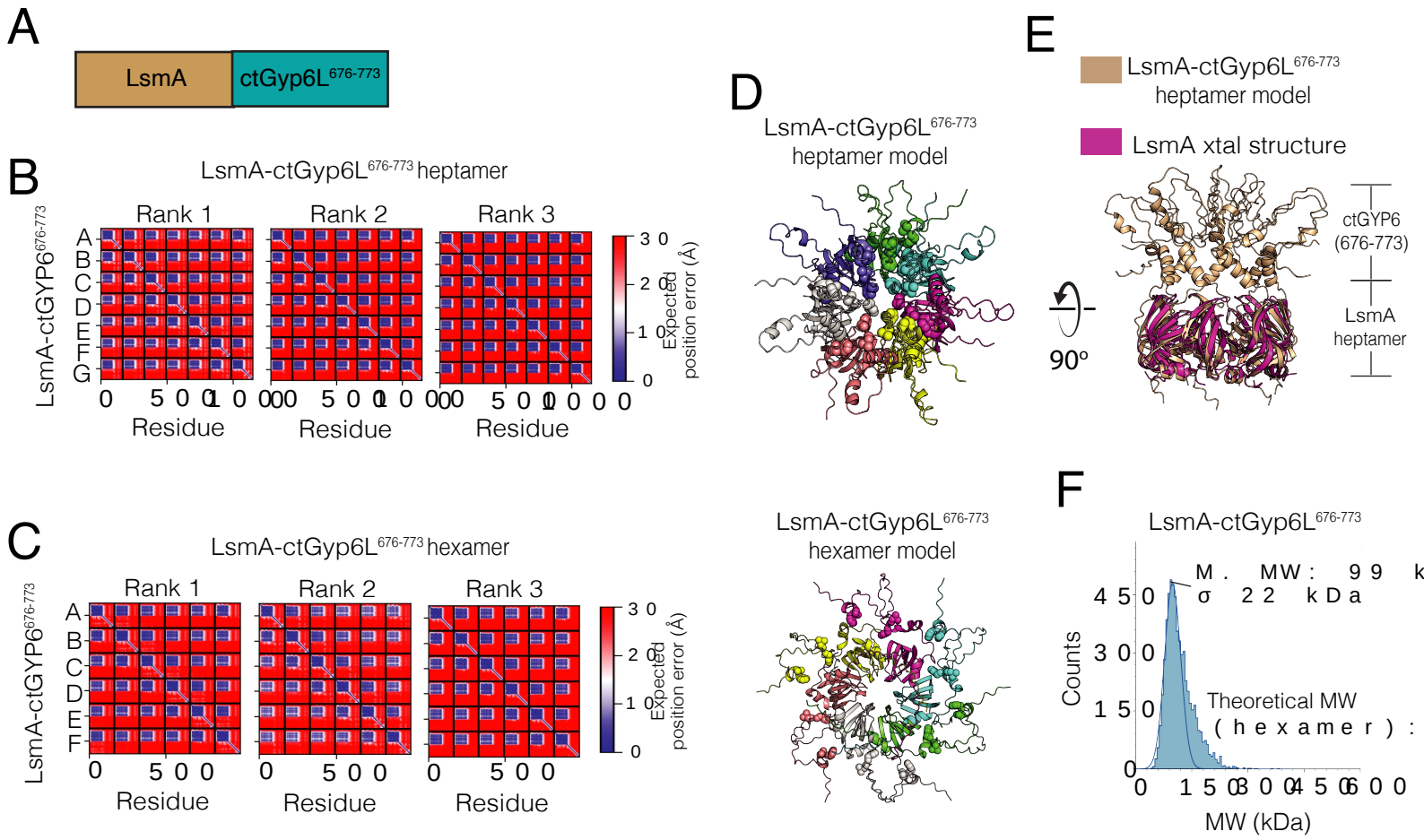

Supplementary Figure 12